CHAPTER–5

Understanding, Modulating and Leveraging Transannular M→Z Interactions

Abstract: Density functional theory calculations have been performed on metallatranes featuring a group 13 element at the bridgehead position to understand the factors that influence the nature of the M····Z (M = Fe, Co, Ni; Z =Al, Ga, In) interaction present in these complexes and the resultant reactivity at the metal center. The strength of the M····Z interaction increases with the increase in the size and polarizability of the bridgehead group 13 elements. The calculated reaction free energies (ΔG° values) for binding of different Lewis bases to the metallatranes are found to be significantly more exergonic for the larger In(III) ions. Quantum theory of atoms in molecules calculations reveal the covalent nature of the M····Z interactions, while the EDA-NOCV analysis indicates the strong binding ability of these metallatranes not only to different σ-donor and π acceptor ligands but also to relatively inert species, such as N_2.

[5.1] Introduction

Transition metal complexes with group 13 elements have attracted considerable interest over the last few decades because of their atypical donor–acceptor interactions in which the transition metal and the ligand play inverted roles [1,2]. Due to the availability of a vacant p orbital, trivalent compounds of group 13 elements can act as σ-acceptor ligands. Therefore, it is not surprising that the first report of a compound featuring coordination of a group 13 element with a transition metal, the $[(C_5H_5)_2WH_2.BF_3]$ complex by Shriver in 1963, involved a W→B interaction [3]. However, the existence of metal-to-boron coordination in the complex was not confirmed by structural characterization, and the actual identity of the system was questioned by Braunschweig and coworkers in the 1990s [4]. The first structurally characterized compound featuring M→Z coordination (**I**, Scheme 5.1; M = transition metal; Z = Lewis acidic group 13 element) was reported in 1979 by Burlitch and Hughes [5], which is also the first example of a metal–alane system. In 1999, Hill and coworkers structurally characterized the $[k^4$-B(mim^{Me})$_3$]Ru(CO)(PPh$_3$) complex (**II**, mim^{Me}=2-mercapto-1-methylimidazolyl) which provided the first definitive evidence for the existence of M→B interaction [6]. Furthermore, in a seminal study, Bourissou and coworkers could successfully isolate a

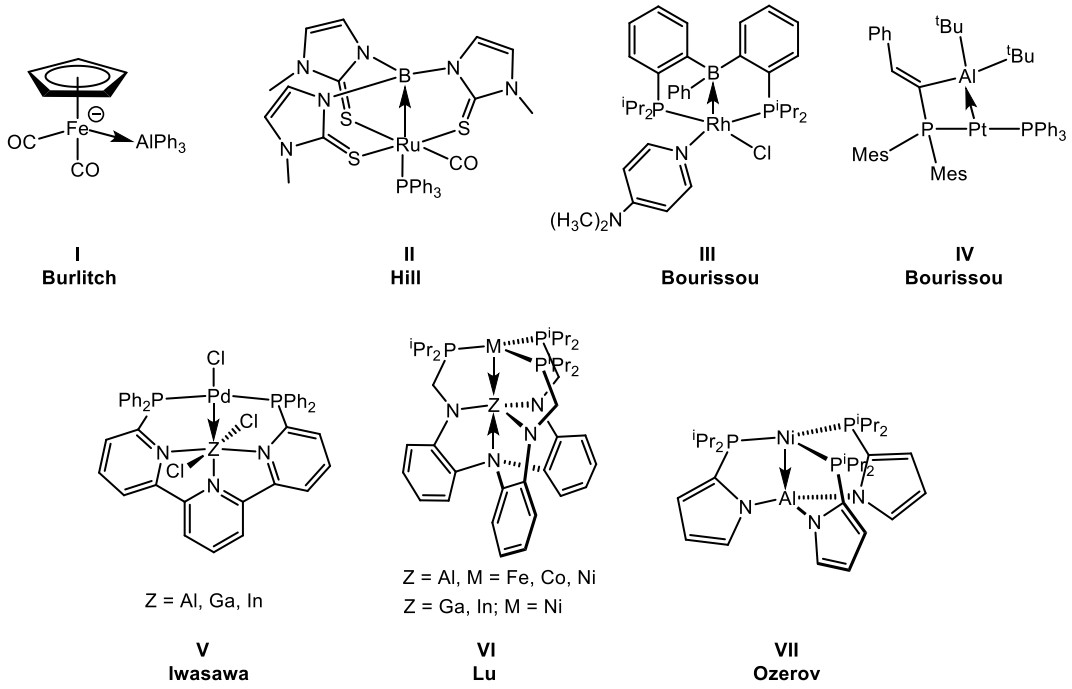

Scheme 5.1: Schematic representation of some of the experimentally accessible transition metal complexes featuring M→Z interaction discussed in this study.

diphosphanylborane supported rhodium complex **III** that exhibits Rh→B interaction which was confirmed by both experimental and computational studies [7].

The development of ambiphilic ligands has led to a renewed interest in the field of M→Z chemistry [8–11]. Interestingly, a majority of the ambiphilic ligands possess boron as σ-acceptor group [12–14] even though a number of those containing its heavier analogs are also known [15–24]. For example, Bourissou and coworkers reported the successful isolation of a four-membered cyclic platinum complex (**IV**) bearing a Pt→Al interaction which can activate enthalpically strong bonds like H–H and N–H under mild reaction conditions [25]. Furthermore, Iwasawa and Takaya used the 6,6″-bis(diphenylphosphino)-2,2′:6′,2″-terpyridine scaffold to support M→Z interaction between Pd and group 13 elements (Al, Ga, and In) (**V**) [26]. Similarly, Lu and coworkers used a double-decker triphosphino(triamido)amine ligand $[N(o\text{-}(NCH_2P(^iPr)_2)C_6H_4)_3]^{3-}$ to support M→Z interaction between first-row late transition metals (Fe, Co, and Ni) and group 13 elements (**VI**) [15,27,28]. In a recent study, Ozerov and coworkers elegantly synthesized a tripodal ligand supported nickel complex (**VII**) featuring a strong Ni→Al interaction and interestingly, **VII** can bind dihydrogen under ambient reaction conditions [24]. These transition metal complexes containing a group 13 element as a σ-acceptor group are commonly known as group 13 metallatranes and feature a transannular M→Z interaction. It is believed that this interaction plays a key role in governing the stability and reactivity of these molecules. Group 13 metallatranes are found to be useful in various catalytic processes, such as dinitrogen activation [29–31], hydrogenation and hydrosilylation of CO_2 [26,32], heterolytic E–H bond activation (E = O, S, C, N) [33–37] and catalytic olefin hydrogenation [15] among others. The flexibility of the M→Z interaction is believed to play a key role in dictating the catalytic activities of group 13 metallatranes. In this work, we perform a comprehensive, in-depth analysis of the nature and strength of the intramolecular transannular interaction present in these molecules aiming at providing valuable information for their use in catalysis and small molecule activation reactions. The transannular M→Z interaction is analyzed as a function of different equatorial (E), apical (L), and Lewis acidic (Z) groups (see Scheme 5.2).

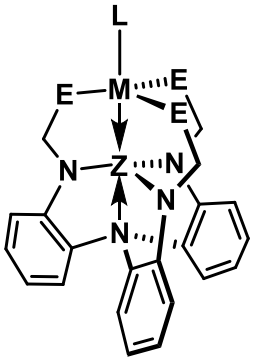

E= S^{i}Pr, P(^{i}Pr)$_2$; M= Fe, Co, Ni; Z= Al, Ga, In

L= NH$_3$, PMe$_3$, N$_2$, CO, NHC, aNHC, CNMe

Scheme 5.2: Schematic representation of the metallatranes considered in this study

A range of L groups has been employed to gain information about the influence of both σ-donor as well as π-acidic groups on the nature of the transannular M→Z interaction (Scheme 5.2). Herein, we use the prefixes phospha and thia for metallatranes with P^{i}Pr$_2$ and S^{i}Pr, respectively, as equatorial groups. Furthermore, the prefixes aluma, galla, and inda are used for metallatranes with Al, Ga, and In as the corresponding Z groups.

[5.2] Computational Details

Density functional theory calculations were employed to optimize all the molecules without any geometrical constraints by using the meta hybrid exchange-correlation energy functional M06 [38] in conjunction with the split valence polarized def2-SVP basis set [39,40] for H, C, N, O, S, and P, and the triple-zeta valence polarized def2-TZVP basis set [39,40] for Fe, Co, Ni, Al, Ga, and In. The core electrons of In were replaced by an effective core potential (ECP). Such a combination of basis sets was found to be useful in the study of inorganic and organometallic compounds [41]. Dispersion effects were incorporated by using the D3 version of Grimme's dispersion correction coupled with the original D3 damping function with the keyword EmpiricalDispersion=GD3 [42]. Frequency calculations were carried out at the same level of theory to check the nature of the stationary points. All the molecules were found to be minima on the potential energy surface as characterized by the presence of only real vibrational frequencies. The ultrafine integration grid was used throughout the calculations. Bonding analyses were performed with the help of the NBO routine [43,44]

as implemented in the Gaussian 09 suite of programs [45]. Furthermore, in order to obtain a comprehensive understanding of the bonding in these molecules, a topological analysis of electron density ρ(r) was carried out with Bader's quantum theory of atoms in molecules (QTAIM) [46-48]. These calculations were done by initially generating the wavefunction files from single point calculations on the optimized geometries, using the same level of theory employed for geometry optimization, and then evaluating these files with the AIMALL program [49].

In order to quantify the bonding interactions of different ligands with the metallatranes studied herein, energy decomposition analysis based on the natural orbitals for chemical valence (EDA-NOCV) [50] calculations were performed on some representative nickelatrane molecules at the Gaussian optimized geometries using the Amsterdam Density Functional (ADF) program [51]. These calculations were carried out at the PBE0-D3/TZ2P level of theory. Scalar relativistic effects were considered by applying the zero-order regular approximation (ZORA) [52]. EDA focuses on the instantaneous interaction energy (ΔE_{int}) associated with the interaction between the donor and acceptor fragments which can be divided into four components: $\Delta E_{int} = \Delta E_{elstat} + \Delta E_{Pauli} + \Delta E_{orb} + \Delta E_{disp}$. The ΔE_{elstat} corresponds to the electrostatic interaction energy between the fragments calculated by means of the frozen electron density distribution of the fragments in the geometry of the molecules. ΔE_{Pauli} refers to the repulsive interactions between the fragments which are caused by the destabilizing interactions between occupied orbitals of both the fragments while ΔE_{orb} and ΔE_{disp} refers, respectively, to the stabilizing orbital and dispersion interactions.

[5.3] Results and Discussion

Molecular geometry: Without any apical substituent (L), the metallatranes studied herein possess pseudo-trigonal mono-pyramidal geometries (Figure 5.1) that changes to pseudo trigonal bipyramidal geometries upon installation of the apical substituent at the transition metal center (TM). Interestingly, all the metallatranes with or without L group possess transannular M····Z (M = Fe, Co or Ni; Z = Al, Ga or In) and Z····N_{apical} interactions, and the extent of these interactions vary depending on the nature of the apical and equatorial substituents. The variations in the extent of M····Z interactions can be described in terms of changes in the pyramidalization angle around the metal (θ_M) and

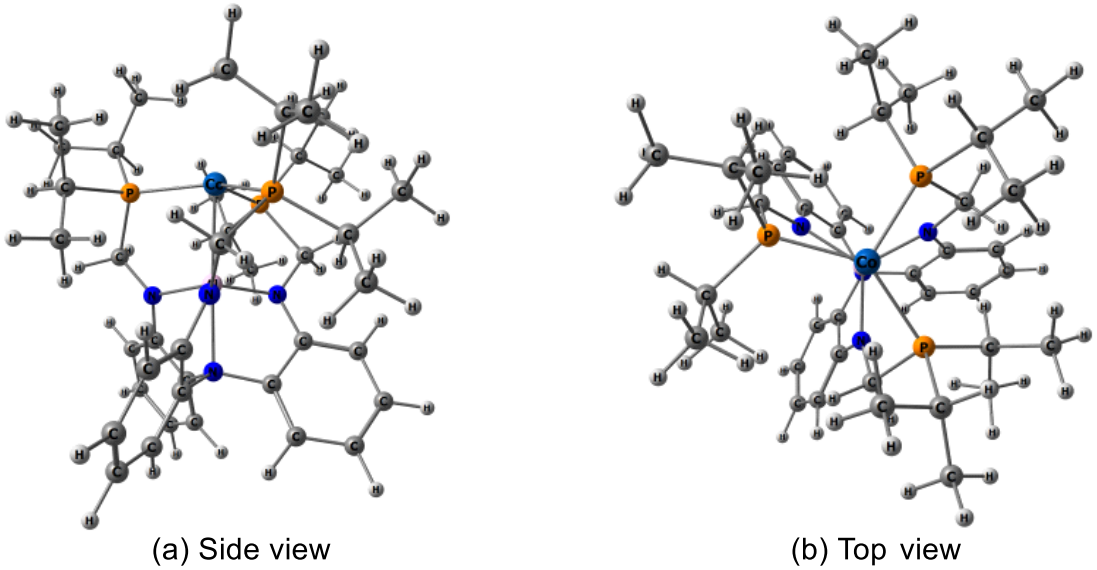

Figure 5.1: Optimized geometry of a representative metallalumatrane (M = Co, E= $^{i}Pr_2$ and Z = Al) molecule given in two different perspectives - (a) side and (b) top view.

the bridgehead group 13 element (θ_Z). The pyramidalization angle refers to the difference in the sum of the angles around M or Z from the regular value of 360°. In all apically substituted metallatranes, the TM and Z centers are found to be pyramidalized outwardly and inwardly, respectively, to a greater extent than those in the parent complex. Usually, a smaller value of θ_M and a higher value of θ_Z provide an ideal condition for a strong M···Z type of interaction as in this case both groups can approach each other appreciably. All the calculated geometrical parameters are given in Tables 5.1–5.3 for nickelatranes, cobaltatranes and iron atranes respectively.

Nickelatranes. Irrespective of the nature of the apical, equatorial or bridgehead groups, all the nickelatrane molecules have singlet ground states. The computed geometrical parameters for the parent phospha-nickelalumatranes (NiP-Al) are found to be in excellent agreement with the experimental values [27]. For example, the computed transannular Ni···Al distance ($d_{Ni\cdots Al}$ = 2.460 Å) is found to be only 0.01 Å shorter than the experimental value (2.450 Å), thereby indicating the reliability of the level of theory used in this study. It is evident from Table 5.1 that, irrespective of the nature of the L group, $d_{Ni\cdots Al}$ increases on incorporation of L at the TM center. This may be attributed to a decrease in the Lewis basicity of the Ni center, thereby weakening the Ni···Al

Table 5.1: Calculated geometrical parameters (transannular M····Al bond distance ($d_{M\cdots Al}$), transannular Al····N_{apical} bond distance ($d_{Al\cdots N_{ap}}$), metal-apical group (L) bond distance ($d_{M\text{-}L}$) in Å, pyramidalization angle at M (θ_M), Al (θ_{Al}) and N_{apical} (θ_N) in degree and natural charge at M (q_M)). Wiberg Bond Index (WBI) values are given in parenthesis. *r*=ratio between M····Al bond distance and the sum of their respective covalent radii.

L	Geometrical parameters	E = P^{i}Pr$_2$			E = S^{i}Pr		
		Ni	Co	Fe	Ni	Co	Fe
–	$d_{M\cdots Al}$	2.460 (0.239)	2.443 (0.286)	2.528 (0.295)	2.426 (0.309)	2.433 (0.360)	2.489 (0.355)
	$d_{Al\cdots N_{ap}}$	2.089 (0.096)	2.136 (0.093)	2.119 (0.095)	2.089 (0.126)	2.124 (0.123)	2.151 (0.306)
	$d_{M\text{-}L}$	-	-	-	-	-	-
	r	1.00	0.99	1.00	0.99	0.99	0.98
	$\theta_M/\theta_{Al}/\theta_N$	3.8/3.4/13.8	5.1/5.6/14.1	6.7/4.9/14.1	1.9/2.9/15.1	3.0/4.4/15.4	4.2/5.8/15.4
	q_M	–0.729	–0.757	–0.633	–0.453	–0.450	–0.362
NH$_3$	$d_{M\cdots Al}$	2.554 (0.285)	2.604 (0.324)	2.647 (0.307)	2.513 (0.367)	2.537 (0.393)	2.636 (0.326)
	$d_{Al\cdots N_{ap}}$	2.192 (0.085)	2.253 (0.082)	2.197 (0.085)	2.192 (0.105)	2.197 (0.098)	2.197 (0.110)
	$d_{M\text{-}L}$	2.153 (0.373)	2.142 (0.374)	2.190 (0.368)	2.166 (0.327)	2.170 (0.340)	2.190 (0.363)
	r	1.04	1.05	1.05	1.03	1.03	1.04
	$\theta_M/\theta_{Al}/\theta_N$	10.0/8.2/13.7	9.7/10.4/13.6	13.9/8.7/13.8	2.5/7.9/14.9	3.9/8.7/15.5	12.2/7.9/15.1
	q_M	–0.927	–0.835	–0.793	–0.619	–0.624	–0.527
PMe$_3$	$d_{M\cdots Al}$	2.674 (0.261)	2.623 (0.301)	2.674 (0.320)	2.776 (0.259)	2.744 (0.298)	2.742 (0.301)
	$d_{Al\cdots N_{ap}}$	2.180 (0.084)	2.266 (0.078)	2.252 (0.078)	2.121 (0.116)	2.156 (0.112)	2.176 (0.111)
	$d_{M\text{-}L}$	2.283 (0.683)	2.296 (0.678)	2.282 (0.733)	2.251 (0.667)	2.270 (0.685)	2.292 (0.704)
	r	1.09	1.06	1.06	1.13	1.11	1.08
	$\theta_M/\theta_{Al}/\theta_N$	14.5/7.2/13.6	12.7/10.3/12.2	17.7/11.6/13.1	20.8/4.0/14.5	19.8/5.7/14.5	17.9/6.7/14.8
	q_M	–1.152	–1.085	–1.071	–0.808	–0.833	–0.823
N$_2$	$d_{M\cdots Al}$	2.640 (0.250)	2.622 (0.286)	2.670 (0.315)	2.682 (0.243)	2.678 (0.282)	2.731 (0.290)
	$d_{Al\cdots N_{ap}}$	2.150 (0.089)	2.182 (0.087)	2.199 (0.085)	2.102 (0.121)	2.129 (0.119)	2.141 (0.120)
	$d_{M\text{-}L}$	1.866 (0.698)	1.855 (0.753)	1.857 (0.815)	1.832 (0.718)	1.844 (0.754)	1.865 (0.790)
	r	1.08	1.06	1.06	1.09	1.08	1.08
	$\theta_M/\theta_{Al}/\theta_N$	11.9/6.3/14.0	13.7/7.8/14.1	14.8/9.2/13.9	15.6/3.3/14.8	15.4/4.5/15.0	15.4/5.2/15.3
	q_M	–0.981	–1.001	–0.789	–0.618	–0.614	–0.510
CO	$d_{M\cdots Al}$	2.689 (0.242)	2.662 (0.276)	2.698 (0.308)	2.789 (0.210)	2.732 (0.271)	2.748 (0.281)
	$d_{Al\cdots N_{ap}}$	2.146 (0.089)	2.177 (0.087)	2.192 (0.085)	2.083 (0.124)	2.133 (0.108)	2.132 (0.122)
	$d_{M\text{-}L}$	1.793 (1.117)	1.792 (1.171)	1.805 (1.251)	1.775 (1.141)	1.799 (1.150)	1.813 (1.226)
	r	1.10	1.08	1.07	1.14	1.11	1.09
	$\theta_M/\theta_{Al}/\theta_N$	13.6/6.0/14.0	14.9/7.4/14.1	15.5/8.9/13.9	19.9/2.6/14.7	14.8/5.0/15.2	16.6/4.7/15.3
	q_M	–1.246	–1.292	–1.095	–0.820	–0.871	–0.791
NHC	$d_{M\cdots Al}$	2.693 (0.275)	2.690 (0.308)	2.822 (0.271)	2.686 (0.318)	2.689 (0.337)	2.706 (0.331)
	$d_{Al\cdots N_{ap}}$	2.211 (0.082)	2.254 (0.078)	2.239 (0.078)	2.168 (0.111)	2.184 (0.109)	2.201 (0.110)
	$d_{M\text{-}L}$	2.074 (0.570)	2.084 (0.658)	2.133 (0.637)	1.971 (0.682)	1.991 (0.709)	2.005 (0.762)
	r	1.10	1.06	1.12	1.10	1.09	1.07
	$\theta_M/\theta_{Al}/\theta_N$	19.4/8.4/13.5	20.3/10.7/13.0	28.0/10.2/13.1	16.8/6.3/15.1	18.7/7.1/14.8	16.0/8.1/15.4
	q_M	–0.926	–0.907	–0.800	–0.704	–0.696	–0.719
aNHC	$d_{M\cdots Al}$	2.618 (0.288)	2.612 (0.315)	2.756 (0.287)	2.614 (0.335)	2.607 (0.358)	2.645 (0.343)
	$d_{Al\cdots N_{ap}}$	2.229 (0.080)	2.270 (0.077)	2.279 (0.076)	2.190 (0.107)	2.206 (0.107)	2.219 (0.106)
	$d_{M\text{-}L}$	2.031 (0.651)	2.036 (0.668)	2.102 (0.626)	1.973 (0.648)	1.989 (0.682)	2.014 (0.712)
	r	1.07	1.09	1.09	1.07	1.06	1.05
	$\theta_M/\theta_{Al}/\theta_N$	16.1/9.5/13.2	17.2/11.7/12.8	21.6/12.4/13.3	14.9/7.2/14.8	15.6/8.1/14.9	15.4/8.9/15.0
	q_M	–1.043	–1.051	–0.988	–0.756	–0.782	–0.739
CNMe	$d_{M\cdots Al}$	2.641 (0.264)	2.620 (0.296)	2.664 (0.325)	2.674 (0.268)	2.660 (0.312)	2.701 (0.310)
	$d_{Al\cdots N_{ap}}$	2.179 (0.086)	2.205 (0.085)	2.227 (0.081)	2.139 (0.104)	2.170 (0.103)	2.163 (0.116)
	$d_{M\text{-}L}$	1.839 (0.970)	1.840 (1.015)	1.849 (1.094)	1.844 (0.945)	1.851 (0.984)	1.859 (1.069)
	r	1.08	1.06	1.05	1.09	1.08	1.07
	$\theta_M/\theta_{Al}/\theta_N$	12.5/7.5/13.8	14.2/8.9/13.9	15.2/10.7/13.5	14.1/5.2/14.9	12.7/6.8/15.1	15.3/6.1/15.2
	q_M	–1.239	–1.277	–1.095	–0.852	–0.861	–0.776

Table 5.2: Calculated geometrical parameters (transannular M···Ga bond distance ($d_{M\cdots Ga}$), transannular Ga···N_{apical} bond distance ($d_{Ga\cdots N_{ap}}$), metal-apical group (L) bond distance ($d_{M\text{-}L}$) in Å, pyramidalization angle at M (θ_M), Ga (θ_{Ga}) and N_{apical} (θ_N) in degree and natural charge at M (q_M)). Wiberg Bond Index (WBI) values are given in parenthesis. *r*=ratio between M···Ga bond distance and the sum of their respective covalent radii.

L	Geometrical parameters	E = P^{i}Pr$_2$			E = S^{i}Pr		
		Ni	Co	Fe	Ni	Co	Fe
–	$d_{M\cdots Ga}$	2.408 (0.306)	2.402 (0.371)	2.471 (0.380)	2.386 (0.376)	2.399 (0.432)	2.469 (0.427)
	$d_{Ga\cdots N_{ap}}$	2.202 (0.114)	2.259 (0.106)	2.247 (0.109)	2.196 (0.133)	2.238 (0.126)	2.270 (0.115)
	$d_{M\text{-}L}$	-	-	-	-	-	-
	r	0.98	0.97	0.97	0.97	0.97	0.97
	$\theta_M/\theta_{Ga}/\theta_N$	4.5/7.3/11.6	6.2/10.5/11.4	7.8/10.1/11.6	2.2/6.4/13.1	3.6/8.8/13.1	3.5/11.8/11.8
	q_M	–0.704	–0.684	–0.555	–0.420	–0.373	–0.280
NH_3	$d_{M\cdots Ga}$	2.458 (0.378)	2.493 (0.429)	2.534 (0.405)	2.430 (0.461)	2.479 (0.445)	2.503 (0.465)
	$d_{Ga\cdots N_{ap}}$	2.350 (0.089)	2.418 (0.082)	2.359 (0.089)	2.335 (0.101)	2.335 (0.104)	2.369 (0.094)
	$d_{M\text{-}L}$	2.113 (0.392)	2.120 (0.384)	2.168 (0.379)	2.119 (0.354)	2.133 (0.367)	2.172 (0.368)
	r	1.00	1.01	1.00	0.99	1.00	0.99
	$\theta_M/\theta_{Ga}/\theta_N$	10.6/15.5/10.4	9.3/18.7/10.2	14.0/16.5/10.4	2.6/14.7/12.3	9.8/14.1/12.1	7.9/17.6/10.6
	q_M	–0.894	–0.766	–0.751	–0.599	–0.531	–0.495
PMe_3	$d_{M\cdots Ga}$	2.522 (0.357)	2.498 (0.400)	2.541 (0.430)	2.599 (0.364)	2.582 (0.409)	2.595 (0.411)
	$d_{Ga\cdots N_{ap}}$	2.362 (0.085)	2.443 (0.075)	2.430 (0.077)	2.304 (0.105)	2.338 (0.100)	2.350 (0.099)
	$d_{M\text{-}L}$	2.268 (0.692)	2.287 (0.679)	2.275 (0.734)	2.263 (0.655)	2.286 (0.667)	2.299 (0.697)
	r	1.03	1.01	1.00	1.06	1.04	1.02
	$\theta_M/\theta_{Ga}/\theta_N$	14.0/15.9/9.8	12.5/18.6/8.5	16.8/20.8/9.3	16.1/11.9/11.8	14.9/14.3/11.8	15.0/15.0/11.8
	q_M	–1.136	–1.036	–1.030	–0.778	–0.785	–0.799
N_2	$d_{M\cdots Ga}$	2.518 (0.331)	2.507 (0.377)	2.544 (0.412)	2.558 (0.323)	2.551 (0.375)	2.596 (0.410)
	$d_{Ga\cdots N_{ap}}$	2.302 (0.096)	2.337 (0.092)	2.363 (0.087)	2.244 (0.119)	2.279 (0.114)	2.306 (0.105)
	$d_{M\text{-}L}$	1.857 (0.697)	1.851 (0.745)	1.855 (0.806)	1.835 (0.703)	1.849 (0.734)	1.870 (0.767)
	r	1.02	1.01	1.00	1.04	1.03	1.02
	$\theta_M/\theta_{Ga}/\theta_N$	11.4/13.0/11.0	13.2/15.0/10.9	14.1/17.3/10.4	13.1/8.6/12.6	12.4/10.8/12.6	10.1/13.9/11.3
	q_M	–0.964	–0.965	–0.758	–0.604	–0.588	–0.471
CO	$d_{M\cdots Ga}$	2.549 (0.325)	2.531 (0.368)	2.563 (0.408)	2.634 (0.292)	2.579 (0.369)	2.605 (0.411)
	$d_{Ga\cdots N_{ap}}$	2.301 (0.095)	2.332 (0.093)	2.359 (0.087)	2.228 (0.121)	2.285 (0.108)	2.305 (0.101)
	$d_{M\text{-}L}$	1.790 (1.104)	1.791 (1.153)	1.804 (1.231)	1.780 (1.116)	1.804 (1.121)	1.826 (1.173)
	r	1.04	1.02	1.01	1.07	1.04	1.03
	$\theta_M/\theta_{Ga}/\theta_N$	12.6/13.0/11.1	14.1/14.6/11.0	14.5/17.1/10.5	16.2/7.8/12.7	12.1/11.7/12.6	12.0/14.1/11.0
	q_M	–1.236	–1.269	–1.074	–0.818	–0.863	–0.743
NHC	$d_{M\cdots Ga}$	2.540 (0.381)	2.543 (0.418)	2.633 (0.381)	2.536 (0.423)	2.548 (0.443)	2.566 (0.441)
	$d_{Ga\cdots N_{ap}}$	2.421 (0.078)	2.455 (0.074)	2.457 (0.074)	2.337 (0.102)	2.356 (0.099)	2.360 (0.101)
	$d_{M\text{-}L}$	2.055 (0.652)	2.069 (0.658)	2.114 (0.649)	1.970 (0.669)	1.993 (0.697)	2.004 (0.755)
	r	1.03	1.03	1.04	1.03	1.03	1.01
	$\theta_M/\theta_{Ga}/\theta_N$	18.9/18.6/9.3	19.7/21.0/8.8	25.7/21.5/8.9	14.0/14.2/12.3	15.8/15.3/11.8	13.8/16.0/12.5
	q_M	–0.879	–0.821	–0.767	–0.660	–0.656	–0.707
aNHC	$d_{M\cdots Ga}$	2.491 (0.389)	2.496 (0.424)	2.601 (0.391)	2.494 (0.435)	2.496 (0.458)	2.526 (0.454)
	$d_{Ga\cdots N_{ap}}$	2.415 (0.079)	2.441 (0.076)	2.463 (0.074)	2.349 (0.099)	2.358 (0.099)	2.377 (0.097)
	$d_{M\text{-}L}$	2.012 (0.658)	2.022 (0.671)	2.088 (0.636)	1.963 (0.649)	1.984 (0.679)	2.007 (0.713)
	r	1.01	1.01	1.02	1.01	1.01	0.99
	$\theta_M/\theta_{Ga}/\theta_N$	16.1/18.5/9.2	16.8/20.4/9.1	20.1/22.1/9.5	13.1/14.7/12.0	14.1/15.3/12.0	13.7/16.6/12.0
	q_M	–1.000	–0.983	–0.960	–0.717	–0.743	–0.723
CNMe	$d_{M\cdots Ga}$	2.509 (0.354)	2.503 (0.395)	2.538 (0.431)	2.538 (0.361)	2.530 (0.412)	2.592 (0.410)
	$d_{Ga\cdots N_{ap}}$	2.337 (0.090)	2.376 (0.085)	2.397 (0.081)	2.290 (0.105)	2.320 (0.102)	2.319 (0.108)
	$d_{M\text{-}L}$	1.835 (0.960)	1.838 (1.001)	1.848 (0.621)	1.845 (0.926)	1.855 (0.960)	1.863 (1.037)
	r	1.02	1.01	1.00	1.03	1.02	1.02
	$\theta_M/\theta_{Ga}/\theta_N$	11.9/14.9/10.6	13.4/17.1/10.1	14.4/19.2/9.9	12.1/11.8/12.2	10.9/13.8/12.3	13.5/13.4/12.7
	q_M	–1.218	–1.241	–1.059	–0.839	–0.837	–0.770

Table 5.3: Calculated geometrical parameters (transannular M···In bond distance ($d_{M\cdots In}$), transannular In···N_{apical} bond distance ($d_{In\cdots Nap}$), metal-apical group (L) bond distance ($d_{M\text{-}L}$) in Å, pyramidalization angle at M (θ_M), In (θ_{In}) and N_{apical} (θ_N) in degree and natural charge at M (q_M)). Wiberg Bond Index (WBI) values are given in parenthesis. *r*=ratio between M···In bond distance and the sum of their respective covalent radii.

L	Geometrical parameters	E = P^{i}Pr$_2$			E = S^{i}Pr		
		Ni	Co	Fe	Ni	Co	Fe
-	$d_{M\cdots In}$	2.461 (0.328)	2.501 (0.374)	2.589 (0.337)	2.453 (0.419)	2.487 (0.456)	2.525 (0.441)
	$d_{In\cdots Nap}$	2.328 (0.107)	2.360 (0.107)	2.376 (0.100)	2.328 (0.141)	2.341 (0.130)	2.343 (0.142)
	$d_{M\text{-}L}$	-	-	-	-	-	-
	r	0.93	0.93	0.94	0.92	0.93	0.92
	$\theta_M/\theta_{In}/\theta_N$	7.9/13.3/10.7	6.5/15.4/12.3	14.3/16.8/12.2	4.6/12.2/12.6	6.2/14.4/12.2	6.2/14.4/13.3
	q_M	–0.650	–0.637	–0.534	–0.384	–0.288	–0.265
NH_3	$d_{M\cdots In}$	2.521 (0.378)	2.553 (0.404)	2.639 (0.367)	2.462 (0.467)	2.528 (0.501)	2.572 (0.441)
	$d_{In\cdots Nap}$	2.411 (0.092)	2.422 (0.089)	2.436 (0.087)	2.365 (0.117)	2.390 (0.133)	2.389 (0.105)
	$d_{M\text{-}L}$	2.074 (0.396)	2.094 (0.396)	2.122 (0.388)	2.078 (0.363)	2.099 (0.368)	2.135 (0.364)
	r	0.95	0.95	0.96	0.93	0.94	0.94
	$\theta_M/\theta_{In}/\theta_N$	13.8/20.3/11.0	15.3/21.4/11.2	21.6/22.9/11.0	5.9/17.714.0	8.2/18.2/14.3	10.0/19.7/12.6
	q_M	–0.831	–0.792	–0.738	–0.638	–0.502	–0.531
PMe_3	$d_{M\cdots In}$	2.561 (0.353)	2.570 (0.389)	2.616 (0.405)	2.509 (0.426)	2.506 (0.488)	2.606 (0.464)
	$d_{In\cdots Nap}$	2.422 (0.086)	2.446 (0.085)	2.437 (0.082)	2.373 (0.111)	2.367 (0.112)	2.386 (0.132)
	$d_{M\text{-}L}$	2.239 (0.686)	2.257 (0.674)	2.263 (0.716)	2.227 (0.660)	2.365 (0.666)	2.260 (0.715)
	r	0.96	0.96	0.95	0.94	0.94	0.95
	$\theta_M/\theta_{In}/\theta_N$	17.5/21.2/10.8	15.2/21.0/12.0	19.7/23.3/11.3	7.8/18.5/14.0	7.2/18.8/14.2	12.7/18.7/14.4
	q_M	–1.062	–0.971	–0.952	–0.917	–0.863	–0.852
N_2	$d_{M\cdots In}$	2.554 (0.335)	2.577 (0.370)	2.615 (0.398)	2.519 (0.397)	2.581 (0.431)	2.603 (0.452)
	$d_{In\cdots Nap}$	2.393 (0.094)	2.407 (0.092)	2.406 (0.090)	2.363 (0.116)	2.379 (0.135)	2.350 (0.128)
	$d_{M\text{-}L}$	1.834 (0.709)	1.836 (0.749)	1.845 (0.802)	1.870 (0.634)	1.844 (0.712)	1.851 (0.784)
	r	0.96	0.96	0.95	0.95	0.96	0.95
	$\theta_M/\theta_{In}/\theta_N$	14.6/18.9/11.2	15.8/20.0/11.3	16.8/20.9/11.7	7.8/17.0/14.1	11.1/16.6/13.9	12.2/18.5/12.2
	q_M	–0.902	–0.885	–0.694	–0.665	–0.554	–0.491
CO	$d_{M\cdots In}$	2.577 (0.327)	2.592 (0.358)	2.626 (0.391)	2.607 (0.370)	2.609 (0.397)	2.616 (0.450)
	$d_{In\cdots Nap}$	2.395 (0.092)	2.405 (0.090)	2.406 (0.088)	2.382 (0.132)	2.378 (0.122)	2.367 (0.120)
	$d_{M\text{-}L}$	1.778 (1.102)	1.783 (1.150)	1.799 (1.221)	1.780 (1.070)	1.794 (1.115)	1.816 (1.168)
	r	0.97	0.97	0.96	0.98	0.97	0.95
	$\theta_M/\theta_{In}/\theta_N$	15.3/19.0/11.3	16.4/19.8/11.4	17.3/20.7/11.7	11.0/16.5/14.3	14.4/17.3/12.8	11.6/19.5/11.8
	q_M	–1.166	–1.177	–0.998	–0.777	–0.795	–0.743
NHC	$d_{M\cdots In}$	2.624 (0.389)	2.583 (0.403)	2.681 (0.368)	2.529 (0.464)	2.582 (0.482)	2.609 (0.467)
	$d_{In\cdots Nap}$	2.461 (0.089)	2.448 (0.082)	2.470 (0.078)	2.400 (0.100)	2.400 (0.128)	2.397 (0.130)
	$d_{M\text{-}L}$	2.019 (0.658)	2.015 (0.665)	2.085 (0.644)	1.980 (0.640)	1.973 (0.682)	1.990 (0.740)
	r	0.99	0.96	0.98	0.95	0.96	0.95
	$\theta_M/\theta_{In}/\theta_N$	13.4/23.4/13.6	21.0/22.9/11.9	29.0/25.1/10.9	9.4/21.1/14.1	14.4/19.0/13.8	14.1/19.0/14.0
	q_M	–0.911	–0.752	–0.635	–0.704	–0.609	–0.641
aNHC	$d_{M\cdots In}$	2.553 (0.376)	2.570 (0.407)	2.650 (0.378)	2.499 (0.478)	2.561 (0.489)	2.592 (0.479)
	$d_{In\cdots Nap}$	2.439 (0.085)	2.442 (0.083)	2.461 (0.085)	2.390 (0.107)	2.398 (0.127)	2.405 (0.127)
	$d_{M\text{-}L}$	1.983 (0.649)	2.000 (0.656)	2.070 (0.633)	1.975 (0.620)	1.969 (0.660)	1.997 (0.695)
	r	0.96	0.96	0.97	0.94	0.96	0.95
	$\theta_M/\theta_{In}/\theta_N$	19.6/22.0/10.9	19.7/22.8/11.0	22.2/24.4/11.7	7.6/19.8/14.8	15.2/18.7/13.2	14.3/19.5/13.6
	q_M	–0.901	–0.859	–0.879	–0.758	–0.635	–0.626
CNMe	$d_{M\cdots In}$	2.556 (0.345)	2.574 (0.380)	2.610 (0.409)	2.570 (0.415)	2.581 (0.437)	2.609 (0.458)
	$d_{In\cdots Nap}$	2.407 (0.090)	2.416 (0.089)	2.418 (0.086)	2.396 (0.129)	2.388 (0.120)	2.382 (0.135)
	$d_{M\text{-}L}$	1.821 (0.957)	1.829 (0.996)	1.842 (1.066)	1.827 (0.913)	1.842 (0.955)	1.857 (1.020)
	r	0.96	0.96	0.95	0.97	0.96	0.95
	$\theta_M/\theta_{In}/\theta_N$	14.6/19.9/11.3	15.9/20.8/11.3	17.1/21.8/11.7	9.8/17.8/14.3	13.3/18.4/12.8	11.7/17.4/14.1
	q_M	–1.139	–1.142	–0.973	–0.752	–0.754	–0.724

interaction. For example, with the insertion of π-acidic apical groups, such as CO, CNMe, and N_2, the $d_{Ni\cdots Al}$ value increases significantly ($d_{Ni\cdots Al}$ = 2.689 Å, 2.641 Å and 2.640 Å for CO, CNMe, and N_2 respectively) compared to that of the parent complex (2.460 Å). Presumably, the Ni→L backbonding outcompetes the Ni····Al interaction, which results in elongation of $d_{Ni\cdots Al}$. Furthermore, among these π-acidic apical groups, the longest $d_{Ni\cdots Al}$ value is obtained for L = CO, which may be attributed to the higher π-acidity of CO compared to CNMe and N_2. Surprisingly, the Ni····Al interaction is weakened even on incorporation of σ-donor L groups like PMe_3 (2.674 Å) and NH_3 (2.554 Å). This is quite interesting as these ligands are expected to enhance the Lewis basicity of the metal center, which should result in a stronger Ni····Al interaction. However, a search of NBO based second order perturbation analysis shows a significant electron density delocalization from the Ni center to the σ^*_{Ni-P} orbitals (Table 5.4), thereby reducing its Lewis basicity which subsequently results in a weaker Ni····Al interaction. Furthermore, between these two σ-donor ligands, the longer $d_{Ni\cdots Al}$ is

Table 5.4: Calculated average stabilization energies (in kcal mol^{-1}) corresponding to the $\sigma_{Ni}\rightarrow\sigma^*_{Ni-P}$ interaction in the nickelatrane complexes.

Apical Groups (L)	**NiP-Al**	**NiP-Ga**	**NiP-In**
	$\sigma_{Ni}\rightarrow\sigma^*_{Ni-P}$	$\sigma_{Ni}\rightarrow\sigma^*_{Ni-P}$	$\sigma_{Ni}\rightarrow\sigma^*_{Ni-P}$
Nil	2.47	2.32	6.38
NH_3	5.70	4.65	12.52
PMe_3	4.57	2.54	9.89
N_2	1.97	3.24	4.55
CO	1.47	5.32	3.24
NHC	3.41	5.19	19.15
aNHC	3.15	5.32	18.05
CNMe	1.44	2.50	4.91

obtained for the PMe_3-substituted NiP-Al complex, which may be attributed to a higher degree of pyramidalization around the Ni center (θ_{Ni}) in this system (14.5°) than that in the corresponding NH_3-substituted compound (10.0°). Similar results were also obtained for strong σ-donor groups like NHC and aNHC as apical groups. However, the $d_{Ni\cdots Al}$ with aNHC (2.618 Å) is computed to be significantly shorter than that with NHC (2.693 Å). Interestingly, N_2, which is a much poorer donor than PMe_3, computes a shorter

$d_{Ni\cdots Al}$ value than that for PMe_3 as the apical group, which may be reasoned not only to the higher degree of pyramidalization at the Ni center for L = PMe_3 (θ_{Ni}=14.5°) than for L = N_2 (θ_{Ni}=11.9°) but also to a higher Ni→σ*$_{Ni–P}$ delocalization in the former than that in the latter (Ni→σ*$_{Ni–P}$ values of 4.57 and 1.97 kcal mol^{-1} for L = PMe_3 and N_2 respectively, see Table 5.4).

For thia-nickelalumatrane (NiS-Al) complexes, the $d_{Ni\cdots Al}$ value in the parent complex (2.426 Å) is found to be shorter than that of its phosphorous analog (2.460 Å), which may be attributed to the greater Lewis basicity of the Ni center in NiS complexes. This is due to delocalization of electron density from the lone pair at the equatorial sulphur atoms to formally vacant Ni orbitals. Furthermore, the Ni···Al interaction in thia-nickelalumatrane shows a trend similar to that in NiP-Al complexes i.e., on insertion of π-acidic apical groups, $d_{Ni\cdots Al}$ increases considerably ($d_{Ni\cdots Al}$= 2.674-2.789 Å), and the increase is more prominent than those of the phosphorus analogs. This may be attributed to a reduced steric crowding in the sulfur analogs, thereby enabling the apical groups to interact more efficiently with the Ni center as compared to their sterically encumbered phosphorus analogs. This leads to an enhancement of the Ni→L (π-acid) backbonding, resulting in a weaker Ni···Al interaction. Similarly, shorter $d_{Ni\cdots Al}$ values are anticipated for σ-donor apical groups in comparison to their phosphorus analogs and, indeed, a shorter $d_{Ni\cdots Al}$ is computed for the NH_3-substituted NiS-Al complex. However, this correlation does not hold for the PMe_3 group and, despite its strong σ-donation ability, a longer $d_{Ni\cdots Al}$ is obtained (2.776 Å) compared to its phosphorus analogs. This may be attributed to a higher value of θ_{Ni} (20.8°) in the NiS-Al complex than that in the corresponding NiP-Al complex (14.5°). Furthermore, $d_{Ni\cdots Al}$ increases with an increase in the value of θ_{Ni} and, indeed, we obtained a reasonable and nice correlation between calculated $d_{Ni\cdots Al}$ and θ_{Ni} values for the NiP-Al (R^2 = 0.76) and NiS-Al (R^2 = 0.92) complexes respectively (Figure 5.2).

Next, we sought to gain information about the nature of the Al···N$_{apical}$ interaction which is also present in these complexes. One might expect that electron density from both the TM center and the N$_{apical}$ group compete for the vacant 3p orbital of Al. So, if one interaction gets stronger, then the other gets weaker and vice versa. However, it is noteworthy to mention that the Al···N$_{apical}$ interaction also gets weakened upon the incorporation of apical groups. For example, all the Al···N$_{apical}$ bond distances

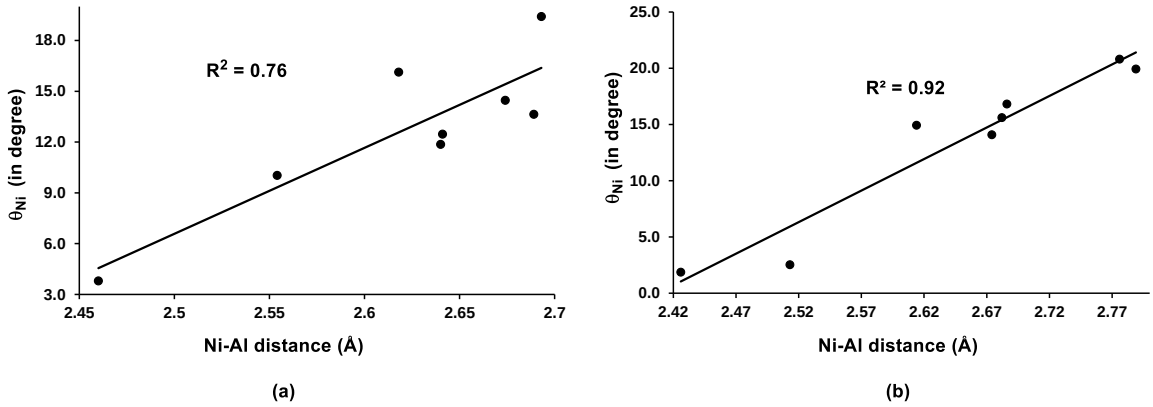

Figure 5.2: Correlation plot between the calculated transannular Ni····Al distances (in Å) and the pyramidalization angle around the TM center (θ_{Ni}, in degree) for the (a) phospha-nickelalumatranes (NiP-Al) and (b) thia-nickelalumatranes (NiS-Al) complexes.

($d_{Al\cdots N_{ap}}$= 2.146-2.229 Å) computed in apically substituted NiP-Al complexes are considerably elongated with respect to that of the parent system (2.089 Å, Table 5.1). Further, it is evident from Table 5.1 that with the variation of apical as well as equatorial groups, θ_{Al} varies to a greater extent while there is no appreciable change in θ_N. We argue that the presence of benzene rings directly attached to the N_{apical} group restricts its pyramidalization to establish a strong transannular Al····N_{apical} interaction.

The calculated transannular distances for the parent phospha-nickelagallatrane (NiP-Ga) and phospha-nickelaindatrane (NiP-In) complexes are found to be in good agreement with the experimentally observed values ($d_{Ni\cdots Ga}$: expt. 2.379 Å, *ca.* 2.408 Å; $d_{Ni\cdots In}$: expt. 2.457 Å, *ca.* 2.461 Å) [15]. Furthermore, it should be noted that the variations in the $d_{Ni\cdots Ga}$ and $d_{Ni\cdots In}$ values obtained for the apically substituted NiP-Ga and NiP-In complexes follow a trend similar to those obtained for NiP-Al complexes (Tables 5.1–5.3). For example, irrespective of the nature of the L groups, all the apically substituted NiP-Ga and NiP-In complexes compute significantly elongated transannular bond distances ($d_{Ni\cdots Ga}$= 2.458-2.549 Å, $d_{Ni\cdots In}$= 2.521-2.624 Å) from their respective bare complexes for reasons explained earlier (*vide supra*). It is evident from the calculated Wiberg Bond Index (WBI) values (Tables 5.1–5.3) that the heavier nickelatranes (M = Ni; Z = Ga, In) exhibit relatively stronger Ni····Z interaction compared to their lighter analogs which may be attributed to the larger size and polarizability of indium(III) ion than that of aluminium(III) and gallium(III) ions (the

ionic radius (Å) increases down the group: Al (0.535), Ga (0.62) and In (0.80)) [15]. In addition, all the nickelaindatrane complexes exhibit significantly higher θ_Z values than the corresponding nickelaluma- and -gallatrane complexes, thereby providing ideal conditions for stronger Ni····Z interaction.

It is interesting to note that the calculated Ni····Z distances are considerably shorter than the sum of the van der Waals radii of Ni (1.60 Å) and the group 13 atoms (Al = 1.84 Å, Ga = 1.87 Å, and In = 1.93 Å) [53] implying the presence of significant bonding interaction between them. Additionally, we have also calculated the *r* values (*r* = ratio between TM····Z distance and the sum of their respective covalent radii [54]), which can be used as an indicative parameter to characterize the transannular interaction [13]. Generally, for a typical TM····Z interaction, the *r* value ranges from 0.91 to 1.26 Å and it is encouraging to note that the calculated *r* values for the nickelatranes lie within the range of 0.93–1.08 Å, revealing the presence of Ni····Z interaction in all the nickelatrane complexes.

The calculated energies of the donor (HOMO) and acceptor (LUMO) orbitals of the parent nickelatranes are listed in Table 5.5. Generally, the higher the energy of the donor orbital the higher will be its donation ability (Lewis basicity), while the lower the energy of the acceptor orbital the higher will be its accepting ability (Lewis acidity). It is evident from Table 5.5 that the parent nickelatrane complexes with indium as the Z group (NiP-In and NiS-In) exhibit significantly higher accepting ability (E_{LUMO} falls within -1.65 to -1.70 eV) than the nickelatranes with aluminium (E_{LUMO} = -0.96 to -1.07 eV) and gallium (E_{LUMO} = -1.25 to -1.39 eV) as the Z groups. The higher Lewis acidity of the nickel center in nickelaindatranes than that in nickelalumatranes or nickelagallatranes may be attributed to better overlap between the larger and softer In(III) ion with the soft Ni(0) center that makes the nickel center electron deficient [15, 55]. Such a Ni→In(III) driven increased Lewis acidity of the metal center is expected to facilitate binding with Lewis bases. Indeed, calculations using NH_3, PMe_3, aNHC, CO and N_2 as the representative Lewis bases shows higher exergonicity (more negative reaction free energies (ΔG)) upon binding with indium anchored metallatranes than those with either aluminium or gallium (Table 5.6). These findings are in excellent agreement with the recent joint computational and experimental studies of Lu and coworkers where they obtained systematic increase in exergonicity for binding of H_2 and N_2 to the indium based nickelatranes [56]. Furthermore, independent works by Figueroa and Gabbaï

Table 5.5: Calculated energies (in eV) of the donor (E_{HOMO}), acceptor (E_{LUMO}) orbitals (centered at the transition metal center) and the proton affinity values (in kcal mol^{-1}) of the parent metallatranes.

	E_{HOMO}	E_{LUMO}	PA
NiP-Al	-4.79	-1.07	246.4
NiP-Ga	-4.91	-1.39	244.9
NiP-In	-4.96	-1.70	238.0
NiS-Al	-4.39	-0.96	239.3
NiS-Ga	-4.57	-1.25	238.6
NiS-In	-4.84	-1.65	229.1
CoP-Al	-4.90	-1.14	249.7
CoP-Ga	-4.89	-1.53	245.7
CoP-In	-4.81	-1.92	242.2
CoS-Al	-4.96	-1.07	241.8
CoS-Ga	-4.97	-1.46	236.3
CoS-In	-5.03	-1.89	234.4
FeP-Al	-4.92	-1.28	256.0
FeP-Ga	-4.90	-1.68	248.5
FeP-In	-4.78	-1.90	240.0
FeS-Al	-4.94	-1.30	246.7
FeS-Ga	-5.01	-1.75	235.9
FeS-In	-4.98	-2.20	239.6

showed that the installation of a σ-acceptor moiety to a transition metal facilitates the binding of a Lewis base donor at the *trans* metal position [57]. In addition, the calculated natural charges at Ni (q_{Ni}) further corroborate the higher Lewis acidity of the parent nickelaindatrane complexes as they compute significantly less negative q_{Ni} values compared to the ones obtained for the parent nickelaluma- and -gallatrane complexes (Tables 5.1–5.3). For nickelatranes with P^iPr_2 as an equatorial group, the ΔG values are in order N_2<NH_3<PMe_3<aNHC<CO; but in case of Fe, the order is NH_3<N_2<PMe_3<aNHC<CO. Further, we obtained no specific trend of ΔG values for S^iPr

as the equatorial group. However, we could not find any specific reason for such discrepancies in the observed trend. Furthermore, to gauge the basicity of the parent nickelatranes, we have calculated their proton affinity (PA) values, which fall within the range of 229.1–246.4 kcal mol^{-1} (Table 5.5). In general, higher the electron donation

Table 5.6: Calculated reaction free energies (ΔG°, in kcal mol^{-1}) for the binding of Lewis basic L groups (L = NH_3, PMe_3, aNHC, CO and N_2) with the transition metal center (M = Ni, Co and Fe) of the metallatranes.

M	Z	E= P^{i}Pr$_2$					E= S^{i}Pr				
		ΔG° (in kcal mol^{-1})					ΔG° (in kcal mol^{-1})				
		NH_3	**PMe_3**	**aNHC**	**CO**	**N_2**	**NH_3**	**PMe_3**	**aNHC**	**CO**	**N_2**
Ni	**Al**	-3.6	-5.2	-17.9	-23.9	-3.3	-5.9	-6.2	-24.8	-24.0	-6.1
	Ga	-6.9	-9.5	-21.9	-25.2	-5.8	-10.3	-9.0	-29.5	-24.5	-6.5
	In	-11.1	-16.2	-27.4	-29.8	-11.1	-27.3	-37.0	-47.4	-28.4	-21.9
Co	**Al**	8.7	6.2	-21.4	-28.1	-8.5	-9.4	-10.8	-30.8	-31.1	-10.1
	Ga	4.9	2.6	-25.6	-30.4	-10.7	-8.8	-12.0	-33.7	-32.1	-9.8
	In	-16.8	-4.7	-34.6	-36.8	-17.7	-11.3	-31.8	-35.9	-33.7	-10.6
Fe	**Al**	-10.8	-14.8	-22.9	-33.1	-13.8	-9.1	-16.5	-32.8	-35.5	-15.3
	Ga	-12.1	-16.8	-24.9	-34.2	-14.6	-8.9	-16.8	-34.5	-34.0	-13.2
	In	-17.1	-20.9	-31.0	-36.9	-17.3	-28.8	-26.3	-40.5	-41.6	-24.1

ability, higher will be the PA value of the metallatranes under consideration. As anticipated, owing to its lower Lewis acidity (of the metal center), aluminium-based metallatranes consistently yield higher PA values than those with either gallium or indium. However, we did not obtain good correlation between E_{HOMO} and PA values. In addition, it should be noted that the calculated PA values are strongly influenced by the strength of the intramolecular transannular interaction between the TM and the Z groups. In other words, a strong Ni···Z interaction should decrease the Lewis basicity of the metal center and vice versa. In fact, we obtained a good correlation (R^2 = 0.81, Figure 5.3) between

the calculated WBI values of the Ni····Z bonds and the PA values. Therefore, it can be concluded that the intramolecular transannular interaction between the TM and the bridgehead group 13 elements (Z) plays a decisive role in governing the Lewis basicity or acidity of the TM center in nickelatranes. Such transannular interactions could thus be leveraged towards the binding of σ-donor or π-acidic ligands to a given transition metal center. For example, employing a tri(phosphine)borane iron system, Peters and coworkers succeeded in isolating several nitrogenous compounds where the Fe····B interaction was found to play a key role in stabilizing those species [29, 58].

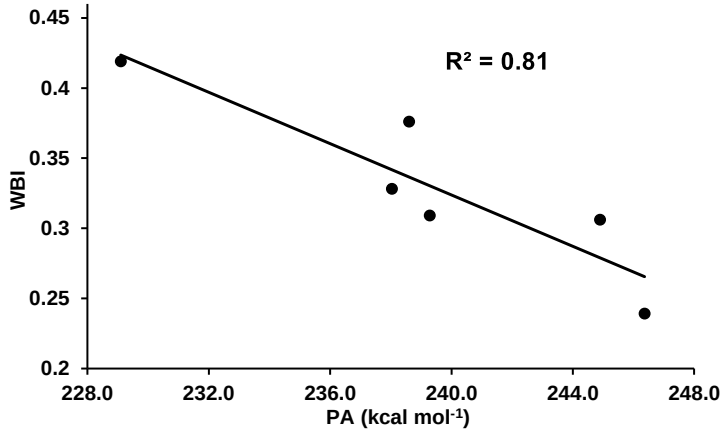

Figure 5.3: Correlation plot between the calculated proton affinity (PA, in kcal mol^{-1}) and WBI values of the Ni····Z (Z = Al, Ga and In) bonds for the parent nickelatranes.

Cobaltatranes. The calculated geometrical parameters for the cobaltalumatranes – all of which have doublet ground state multiplicities – are found to be in excellent agreement with the experimentally observed values. For example, the calculated Co····Al distance in phospha-cobaltalumatrane (CoP-Al) with N_2 as the apical group ($d_{Co\cdots Al}$ = 2.622 Å, Table 5.1) is found to deviate by only 0.002 Å from the experimental value of 2.620 Å [27]. The variations in the $d_{Co\cdots Al}$ values for these apically substituted cobaltalumatranes show a trend similar to that for the phospha-nickelalumatranes. For example, for π-acidic L groups, the $d_{Co\cdots Al}$ values increase significantly from the parent complex, which may be attributed to stronger Co→L backbonding that weakens the Co····Al interaction. Among these three π-acidic groups, the strongest Co····Al interaction is obtained for CNMe, which may be attributed to the lower value of θ_{Co} and a higher value of θ_{Al} (Table 5.1). The $d_{Co\cdots Al}$ distance also gets elongated upon installation of σ-donor groups due to transfer of electron density from filled cobalt orbitals to vacant $\sigma^*_{Co\text{-}P}$ orbitals as

evident from the NBO second-order perturbation analysis (Table 5.7). Further, it is interesting to note that there exist a good correlation between the extent of $Co \rightarrow \sigma^*_{Co\text{-}P}$ interaction with the nature of the ligands attached to the metal center. It is evident from Table 5.7 that the extent of $Co \rightarrow \sigma^*_{Co\text{-}P}$ interaction increases and decreases upon installation of the electron donating (NH_3, PMe_3, NHC and aNHC) and withdrawing (CO, N_2 and CNMe) ligands respectively at the TM center. Furthermore, the weakest Co···Al interaction is obtained for NHC, which may be attributed to the particularly high θ_{Co} value of 20.3º observed in this system (Table 5.1).

Table 5.7: Calculated average stabilization energies (in kcal mol^{-1}) corresponding to the $\sigma_{Co} \rightarrow \sigma^*_{Co\text{-}P}$ interaction in the cobaltatrane complexes.

Apical Groups (L)	**CoP-Al**	**CoP-Ga**	**CoP-In**
	$\sigma_{Co} \rightarrow \sigma^*_{Co\text{-}P}$	$\sigma_{Co} \rightarrow \sigma^*_{Co\text{-}P}$	$\sigma_{Co} \rightarrow \sigma^*_{Co\text{-}P}$
Nil	1.11	0.79	1.85
NH_3	1.21	2.62	2.91
PMe_3	1.07	1.62	3.68
N_2	1.33	1.34	2.30
CO	1.82	1.00	1.55
NHC	1.70	3.20	4.52
aNHC	2.45	3.44	6.49
CNMe	0.91	1.14	2.55

For thia-cobaltalumatrane (CoS-Al) complexes, the $d_{Co\cdots Al}$ with π-acidic ligands were computed to be longer than their corresponding phosphorous analogs. On the other hand, a significantly shorter $d_{Co\cdots Al}$ is obtained for NH_3 (2.537 Å) than that in the corresponding CoP complex (2.604 Å), which may be attributed to smaller pyramidalization at the cobalt center (θ_{Co} = 9.7° and 3.9° for CoP and CoS complexes respectively, Table 5.1). However, we obtained a highly elongated Co···Al bond (weaker Co···Al interaction) for PMe_3 than that in the corresponding CoP complex, which may be attributed not only to the higher value of θ_{Co} but also to a stronger Co–PMe_3 overlap in the CoS complex.

The variations in the geometrical parameters obtained for the phospha-cobaltagallatrane (CoP-Ga) and phospha-cobaltaindatrane (CoP-In) complexes follow a trend similar to that of their lighter analog. In addition, the calculated *r* values for the

cobaltatranes lie within the range of 0.93–1.11 Å, indicating the presence of considerable Co····Z interactions. Furthermore, it should be noted that like the nickelatranes, the heavier cobaltatranes also exhibit relatively stronger Co····Z interactions than their lighter analogs for reasons explained earlier. The metal center in both the parent CoP-In and CoS-In complexes are highly Lewis acidic in nature (more stabilized LUMO, Table 5.5) and hence could effectively bind to electron-donating ligands. For example, the Co–NH_3 distances in phospha- cobaltatranes decrease in the order Al (2.142Å)> Ga (2.120Å)> In (2.094 Å) (Tables 5.1–5.3). Also, the calculated ΔG° values for binding of different Lewis bases are found to systematically increase (more exergonic) in the order Al>Ga>In (Table 5.6). The calculated PA values for the cobaltatranes lie within the range of 234.4–249.7 kcal mol^{-1} with the highest PA values being computed for Co-Al complexes (Table 5.5). Gratifyingly, we obtained a nice correlation (R^2 = 0.91, Figure 5.4) between the calculated WBI values corresponding to the Co····Z interaction and the PA values.

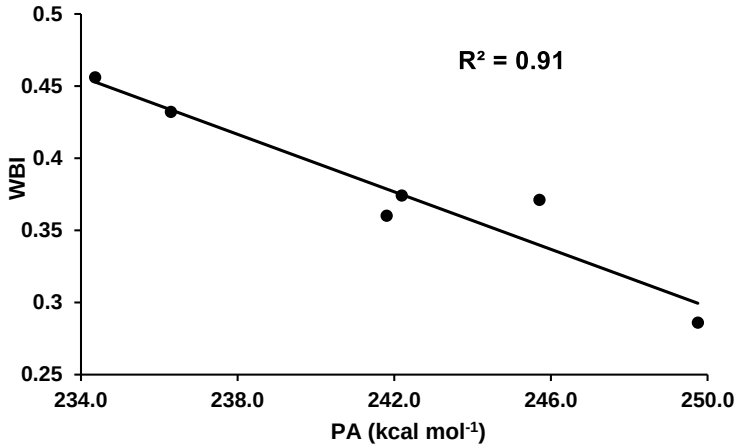

Figure 5.4: Correlation plot between the calculated proton affinity (PA, in kcal mol^{-1}) and WBI values corresponding to the Co····Z (Z = Al, Ga and In) interaction for the parent cobaltatranes.

Iron atranes. Two spin states, viz., singlet and triplet may be envisioned for iron atranes. Computation of the relative energies of both the spin states shows that, irrespective of the nature of the equatorial or apical groups, the triplet states are more stable than the singlet ones by 19.5–33.1 kcal mol^{-1} (Tables 5.8–5.10) [27]. Therefore, only complexes with triplet ground states were considered in this study. Irrespective of the nature of the equatorial groups, the transannular Fe····Al distance for the apically substituted iron alumatranes increase considerably ($d_{Fe\cdots Al}$ values vary from 2.647-2.822 Å and 2.636-2.748 Å for P^iPr_2 and S^iPr as the equatorial groups respectively) in

comparison to that of the parent complex ($d_{Fe\cdots Al}$= 2.528 Å and 2.489 Å for FeP-Al and FeS-Al respectively, Table 5.1). Among the phospha-iron atranes, the longest transannular bond ($d_{Fe\cdots Z}$) is computed for NHC, with this apical group leading to significantly higher θ_{Fe} values than those of the other systems (Tables 5.1–5.3). On the other hand, for the thia-iron atranes, the largest $d_{Fe\cdots Z}$ value is obtained for CO which may be attributed to the formation of the strong Fe–CO bond. NH_3 bound iron atranes compute the shortest Fe····Z distance except for phospha-iron indatranes, for which the one with isonitrile (CNMe) computed the shortest Fe····In distance. Furthermore, akin to nickelatranes and cobaltatranes, we have also obtained a nice correlation between the

Table 5.8: Calculated singlet-triplet energy separation values ($\Delta E_{S\text{-}T}$, in kcal mol^{-1}) for the phospha iron alumatrane (FeP-Al) and thia iron alumatrane (FeS-Al) complexes.

FeP-Al		**FeS-Al**	
L	**$\Delta E_{S\text{-}T}$**	**L**	**$\Delta E_{S\text{-}T}$**
Nil	-24.10	**Nil**	-26.71
NH_3	-25.57	**NH_3**	-24.56
PMe_3	-27.97	**PMe_3**	-20.13
N_2	-22.01	**N_2**	-33.02
CO	-21.92	**CO**	-30.66
NHC	-32.32	**NHC**	-20.28
aNHC	-20.45	**aNHC**	-26.26
CNMe	-20.50	**CNMe**	-27.57

Table 5.9: Calculated singlet-triplet energy separation values ($\Delta E_{S\text{-}T}$, in kcal mol^{-1}) for the phospha iron gallatrane (FeP-Ga) and thia iron gallatrane (FeS-Ga) complexes.

FeP-Ga		**FeS-Ga**	
L	**$\Delta E_{S\text{-}T}$**	**L**	**$\Delta E_{S\text{-}T}$**
Nil	-24.41	**Nil**	-28.24
NH_3	-24.66	**NH_3**	-21.79
PMe_3	-28.75	**PMe_3**	-30.71
N_2	-22.47	**N_2**	-30.11
CO	-21.52	**CO**	-27.78
NHC	-31.38	**NHC**	-29.54
aNHC	-19.53	**aNHC**	-26.29
CNMe	-21.06	**CNMe**	-27.03

Table 5.10: Calculated singlet-triplet energy separation values (ΔE_{S-T}, in kcal mol^{-1}) for the phospha iron indatrane (FeP-In) and thia iron indatrane (FeS-In) complexes.

FeP-In		FeS-In	
L	**ΔE_{S-T}**	**L**	**ΔE_{S-T}**
Nil	-31.43	**Nil**	-30.91
NH_3	-31.13	**NH_3**	-38.44
PMe_3	-31.32	**PMe_3**	-29.32
N_2	-25.66	**N_2**	-31.00
CO	-24.98	**CO**	-31.07
NHC	-30.09	**NHC**	-33.14
aNHC	-25.11	**aNHC**	-30.23
CNMe	-24.83	**CNMe**	-27.88

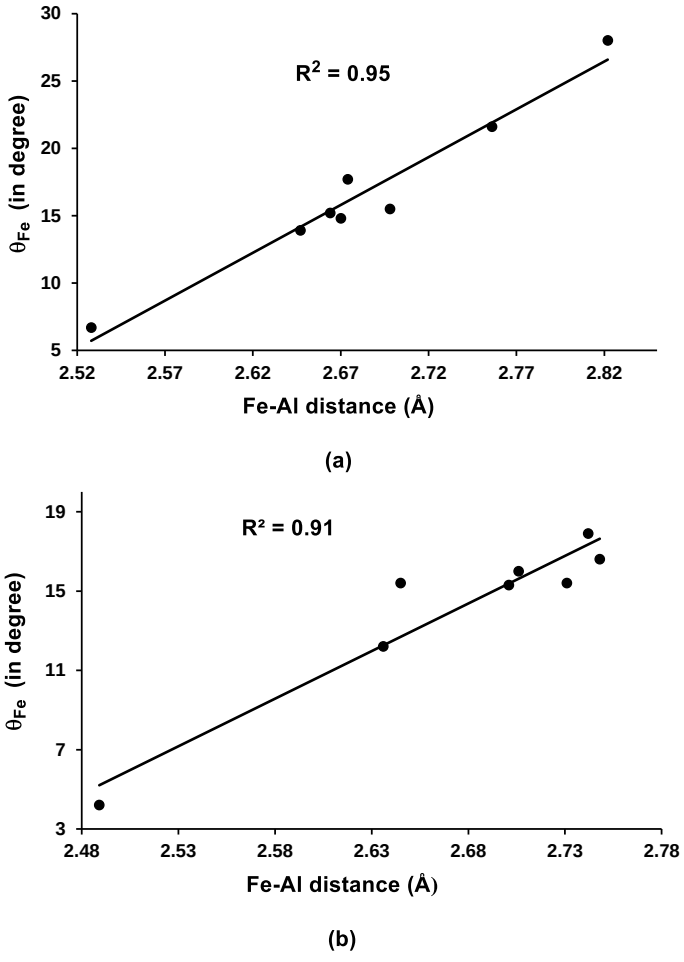

Figure 5.5: Correlation plot between the calculated transannular Fe····Al distances (in Å) and the pyramidalization angle around the TM center (θ_{Fe}, in degree) for the (a) phospha iron alumatranes (FeP-Al) and (b) thia iron alumatranes (FeS-Al) complexes.

calculated transannular Fe····Al distances and the pyramidalization angle around the TM center (θ_M) for the FeP-Al (R^2 = 0.95) and FeS-Al (R^2 = 0.91) complexes (Figure 5.5). The geometrical variations obtained for the iron gallatrane and iron indatrane complexes show a trend similar to those obtained for iron alumatranes. Additionally, the calculated *r* values for the iron atranes lie within 0.92–1.12 Å, indicating the presence of Fe····Z interactions.

In accordance with the trends observed for other atranes, the iron center of both FeP-In and FeS-In complexes are found to be more Lewis acidic compared to their lighter analogs, which is not only evident from their calculated natural charge values (less negative) at the Fe center but also from the calculated energies of their acceptor orbitals (Table 5.5). Such an increase in Lewis acidity of the metal center make it susceptible to attack by Lewis bases. Indeed, calculations indicate stronger binding of Lewis bases (more exergonic $\Delta G°$ values) to the iron atoms of FeP-In and FeS-In complexes than those with their lighter counterparts (Table 5.6). Furthermore, the calculated PA values of these iron atranes lie within 235.9–256.0 kcal mol^{-1} (Table 5.5) with the parent iron alumatranes yielding considerably higher PA values than those obtained for the corresponding gallatranes and indatranes, indicating the relatively higher Lewis basicity of the bare iron alumatrane complexes. These facts once again highlights the importance of M····Z interactions in controlling the reactivity at the metal center.

Furthermore, a comparison of the geometrical parameters for the parent metallatranes (Tables 5.1–5.3) reveals that, irrespective of the nature of Z or E groups, iron atranes exhibit relatively stronger M····Z interactions than either cobaltatranes or nickelatranes. The strengthening of the Fe····Z interactions in the parent iron atranes may be credited to the lower electronegativity of the iron center (χ_{Fe} = 1.83, χ_{Co} = 1.88, and χ_{Ni} = 1.91), which allows the effective delocalization of the electron density from the TM center to the Z groups. However, this correlation does not hold good for some of the apically substituted (L = NH_3, NHC, and aNHC) metallatranes.

In order to understand the influence or role of the transannular M→Z interactions on the stability of the metallatrane complexes studied herein, we performed few representative calculations by removing this interaction, i.e., increasing the distance

between M and Z. Indeed, as anticipated, the presence of transannular M→Z interactions significantly stabilizes the frontier molecular orbitals (shown here for the parent nickelalumatrane as a representative example, Figure 5.6) which is reflected not only in the calculated HOMO-LUMO gaps but also in the stabilization energies obtained from NBO based second order perturbation analysis (Table 5.11).

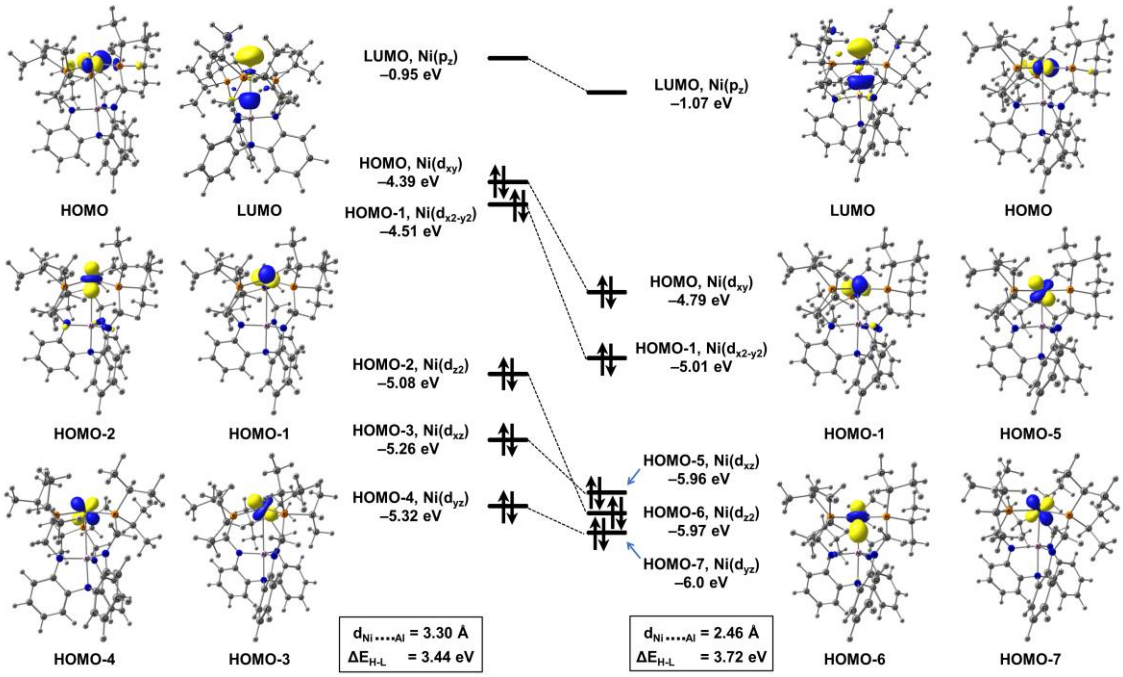

Figure 5.6: Qualitative orbital correlation diagram showing the stabilization of the metal-based molecular orbitals (d-splitting) as a result of increase in Ni→Al interaction of nickelatranes.

Table 5.11: Calculated HOMO-LUMO gap values ($\Delta E_{H\text{-}L}$, in eV) and donor(M)→acceptor(Z) stabilization energies (in kcal mol^{-1}) for the parent NiP-Al, CoP-Al and FeP-Al complexes in their equilibrium and constrained (M-Z=3.3Å) optimized geometry.

Molecules	**Equilibrium M····Z distance**		**M····Z =3.3Å**	
	$\Delta E_{H\text{-}L}$	**donor(M)→acceptor(Al)**	**$\Delta E_{H\text{-}L}$**	**donor(M)→acceptor(Al)**
NiP-Al	3.72	41.17	3.44	3.82
CoP-Al	3.42	14.13	2.62	0.06
FeP-Al	2.61	9.53	2.25	0.18

[5.4] Topological analysis

The AIM analysis can be used as an efficient tool to characterize the weak intramolecular transannular interaction present in a complex in terms of bond path and bond critical points (BCPs). The computed AIM parameters, such as electron density at the bond critical points (BCP, ρ_b), laplacian of electron density at BCP [$\nabla^2\rho$(r)], and the local electronic energy density H(r) can also be useful in determining the nature of chemical bonds. Usually, a covalent (also referred to as shared or open-shell) type of interaction is characterized by a large value of ρ_b (> 0.2 a.u.) and large and negative values of [$\nabla^2\rho$(r)]. In contrast, for closed-shell interactions (e.g., van der Waals, ionic or hydrogen bond interaction), ρ_b is small (< 0.1 a.u.) while its laplacian, [$\nabla^2\rho$(r)] is positive. However, it is always advisable to calculate the electronic energy density H(r) values to get a clear-cut distinction between the open and closed-shell interactions. The local electronic energy density H(r) can be defined as the sum of local potential (V(r)) and kinetic energy (G(r)) densities, i.e. H(r) = V(r) + G(r). Generally, covalent interactions are characterized by negative values of H(r) while ionic or van der Waals interactions have positive values of H(r) [59]. In other words, the magnitude of H(r) reflects the degree of covalency present in a chemical bond within the QTAIM framework. Therefore, some of the covalent bonding interactions, such as polar bonds and donor–acceptor interactions, are associated with a negative value of H(r) and positive values of $\nabla^2\rho$(r). In order to have a measure of the covalent bond order between atoms A and B, the delocalization index DI(A,B) of distinct A and B atom pairs was also calculated.

To get further insight into the nature of the transannular interaction present in the metallatranes considered in this study, we performed QTAIM studies on a few representative metallatranes with a pure σ-donor (NH_3) and π-acceptor (CO) ligands as the apical groups, and the important AIM parameters at the bond critical point (BCP) of the M····Z bonds are listed in Tables 5.12–5.14. The presence of M····Z interactions in all the metallatranes are characterized by the presence of a (3,–1) BCP. In addition, the formation of the (3,+1) ring critical points (RCPs) further corroborates the presence of transannular interactions between the M and Z atoms, as it helps in the formation of five-membered rings in these complexes (Figure 5.7). It should be noted that all the metallatranes exhibit considerable electron density at the M····Z bond critical points that increases with the decrease in the length of transannular M····Z distances. Indeed, we have obtained a nice correlation between the calculated transannular M····Z distances and the electron density at the M····Z BCPs (Figures 5.8–5.10). Irrespective of the nature of the metal atom and the equatorial substituents, the values of electron density (ρ) at the

bond critical point gradually increases with an increase in the size of the Z(III) ions, i.e., ρ increases in the order Al < Ga < In. For example, the values of ρ (in a.u.) for CO bound thia-nickelatranes increases from 0.027 (Al)→ 0.041 (Ga)→ 0.046 (In). The same

Table 5.12: Calculated important AIM parameters such as electron density at the BCP (ρ), laplacian of electron density ($\nabla^2\rho$) and local energy density (H(r)) at the M····Al bond critical points for the metallalumatranes. The delocalization index (DI) values of the M····Al bonds are also tabulated. All values are in a.u.

Apical groups (L)	AIM parameter	E=P^{i}Pr$_2$			E =S^{i}Pr		
		Ni-Al	Co-Al	Fe-Al	Ni-Al	Co-Al	Fe-Al
Nil	ρ	0.037	0.044	0.043	0.040	0.046	0.046
	$\nabla^2\rho$	0.041	0.032	0.012	0.042	0.030	0.09
	H(r)	-0.012	-0.017	-0.017	-0.014	-0.018	-0.019
	DI	0.179	0.238	0.241	0.199	0.247	0.268
NH_3	ρ	0.040	0.041	0.042	0.042	0.044	0.041
	$\nabla^2\rho$	0.017	-0.002	-0.013	0.015	-0.003	-0.011
	H(r)	-0.015	-0.016	-0.017	-0.016	-0.018	-0.016
	DI	0.211	0.247	0.247	0.240	0.272	0.241
CO	ρ	0.032	0.037	0.039	0.027	0.033	0.035
	$\nabla^2\rho$	0.104	0.002	-0.011	0.008	0.002	-0.008
	H(r)	-0.011	-0.014	-0.015	-0.008	-0.009	-0.013
	DI	0.156	0.197	0.224	0.124	0.177	0.189

Table 5.13: Calculated important AIM parameters such as electron density at the BCP (ρ), laplacian of electron density ($\nabla^2\rho$) and local energy density (H(r)) at the M····Ga bond critical points for the metallagallatranes. The delocalization index (DI) values of the M····Ga bonds are also tabulated. All values are in a.u.

Apical groups (L)	AIM parameter	E=P^{i}Pr$_2$			E =S^{i}Pr		
		Ni-Ga	Co-Ga	Fe-Ga	Ni-Ga	Co-Ga	Fe-Ga
Nil	ρ	0.053	0.060	0.058	0.057	0.062	0.057
	$\nabla^2\rho$	0.050	0.035	0.011	0.050	0.028	0.018
	H(r)	-0.018	-0.022	-0.021	-0.019	-0.023	-0.021
	DI	0.433	0.538	0.518	0.473	0.551	0.544
NH_3	ρ	0.056	0.056	0.055	0.059	0.057	0.056
	$\nabla^2\rho$	0.015	0.008	0.001	0.013	0.007	0.011
	H(r)	-0.020	-0.019	-0.019	-0.021	-0.020	-0.019
	DI	0.499	0.546	0.510	0.557	0.531	0.558
CO	ρ	0.048	0.053	0.053	0.041	0.049	0.049
	$\nabla^2\rho$	0.011	0.007	0.004	0.008	0.003	0.002
	H(r)	-0.016	-0.018	-0.036	-0.013	-0.016	-0.016
	DI	0.390	0.454	0.481	0.330	0.428	0.453

Table 5.14: Calculated important AIM parameters such as electron density at the BCP (ρ), laplacian of electron density ($\nabla^2\rho$) and local energy density (H(r)) at the M···In bond critical points for the metallaindatranes. The delocalization index (DI) values of the M···In bond are also tabulated. All values are in a.u.

Apical groups (L)	AIM parameter	E=P^{i}Pr$_2$			E =S^{i}Pr		
		Ni-In	Co-In	Fe-In	Ni-In	Co-In	Fe-In
Nil	ρ	0.057	0.056	0.051	0.058	0.059	0.056
	$\nabla^2\rho$	0.112	0.090	0.063	0.111	0.086	0.076
	H(r)	-0.014	-0.015	-0.013	-0.015	-0.017	-0.016
	DI	0.510	0.574	0.522	0.553	0.595	0.583
NH$_3$	ρ	0.055	0.054	0.048	0.061	0.056	0.054
	$\nabla^2\rho$	0.071	0.062	0.046	0.086	0.064	0.052
	H(r)	-0.015	-0.015	-0.012	-0.017	-0.016	-0.015
	DI	0.532	0.553	0.501	0.591	0.588	0.545
CO	ρ	0.049	0.050	0.050	0.046	0.049	0.050
	$\nabla^2\rho$	0.062	0.056	0.047	0.054	0.051	0.047
	H(r)	-0.012	-0.013	-0.013	-0.011	-0.013	-0.013
	DI	0.430	0.473	0.490	0.421	0.461	0.497

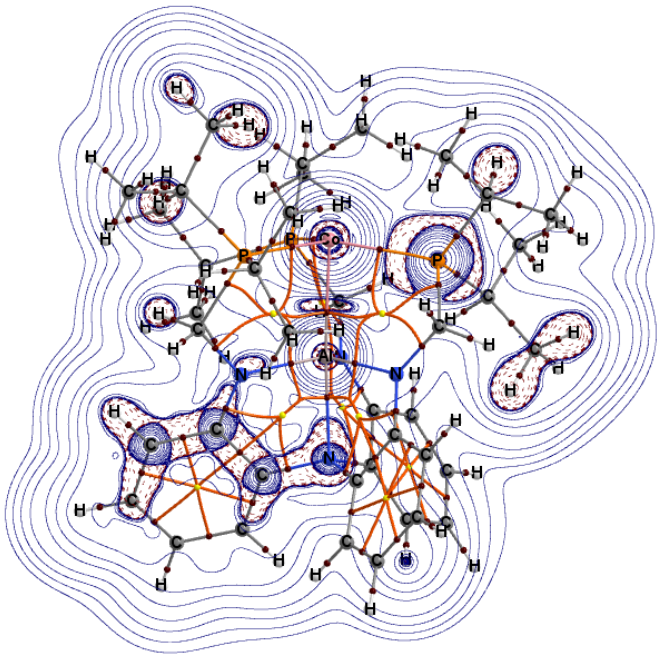

Figure 5.7: Contour line diagram $\nabla^2\rho$ (r) for a representative metallatrane molecule (CoP-Al) in the P-Co-Al plane. The solid lines joining the atomic nuclei are the bond paths whereas the bond critical points and the ring critical points are denoted by the brown and yellow color spheres respectively. The solid blue lines represents the regions of charge depletion ($\nabla^2\rho$ >0) whereas the dashed red lines represent the regions of charge concentration ($\nabla^2\rho$ <0).

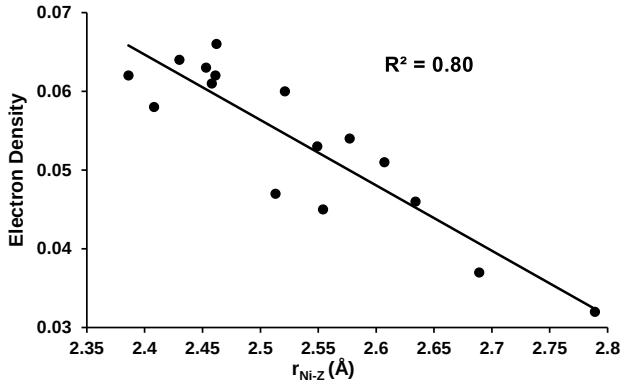

Figure 5.8: Correlation plot between the transannular Ni····Z (Z = Al, Ga and In) bond distances and electron density at the bond critical point of the Ni····Z bonds for the nickelatranes (Omitting the points corresponding to the parent NiP-Al and NiS-Al complexes).

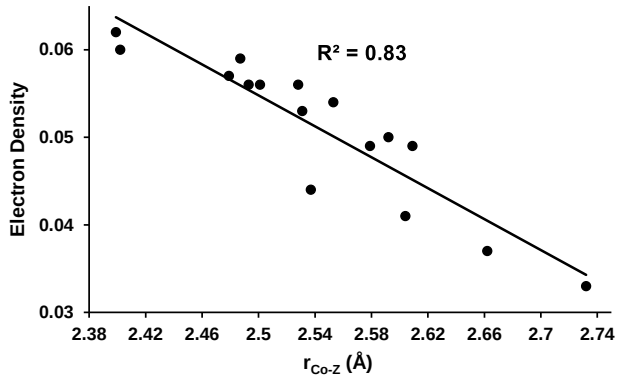

Figure 5.9: Correlation plot between the transannular Co····Z (Z = Al, Ga and In) bond distances and electron density at the bond critical point of the Co····Z bonds for the cobaltatranes (Omitting the points corresponding to the parent CoP-Al and CoS-Al complexes).

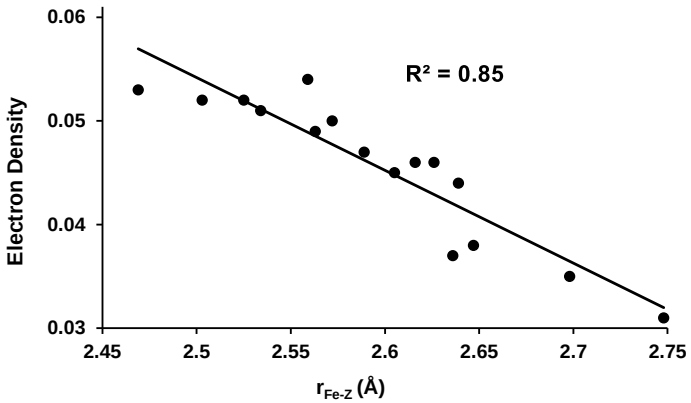

Figure 5.10: Correlation plot between the transannular Fe····Z (Z = Al, Ga and In) bond distances and electron density at the bond critical point of the Fe····Z bonds for the iron atranes (Omitting the point corresponding to the parent FeS-Al complexe).

is true for the calculated delocalization index (DI) values. However, we did not notice any appreciable changes in the values of the energy density *H*(r) by varying either the

metal or the group 13 elements. The calculated $H(r)$ values vary from –0.008 to –0.023, indicating the presence of considerable covalent character in the transannular bonds (M→Z) of the metallatranes considered in this study.

[5.5] EDA-NOCV Analysis

Finally, we investigated the M–L (M = Ni; L = NH_3, NHC, N_2, CO) bonding interactions of the distinct Z-bearing (Z = Al, Ga, In) phospha-nickelatrane complexes within the EDA-NOCV approach [50]. For that, the interaction energy (ΔE_{int}) between two fragments – in our case the naked metallatranes and the apical ligands L – is decomposed into physically meaningful contributions (ΔE_{elstat}, ΔE_{Pauli}, ΔE_{orb}, and ΔE_{disp}, *vide supra*). The ΔE_{orb} term is then partitioned into contributions coming from the distinct NOCV pairs. All the energy values are shown in Table 5.15, while Figure 5.11

Table 5.15: EDA-NOCV Results (PBE0-D3/TZ2P) for the Nickela-Phosphatrane Systems Calculated in this Work. Energy Terms are given in kcal mol^{-1}. For ΔE_{disp}, ΔE_{elstat}, and ΔE_{orb}, the Values in Parentheses Show the Weight of each Contribution with Respect to the Total Attractive Interaction. For the σ, $\pi_{\parallel}$, $\pi_{\perp}$, and Rest Terms associated with ΔE_{orb}, the Values in Parentheses Show the Weight of Each Contribution with respect to the Total Orbital Interaction, ΔE_{orb}.

System	ΔE_{int}	ΔE_{Pauli}	ΔE_{disp}	ΔE_{elstat}	ΔE_{orb}	ΔE_{orb} σ	ΔE_{orb} $\pi_{\parallel}$	ΔE_{orb} $\pi_{\perp}$	ΔE_{orb} rest
NiP-Al-NH_3	-19.1	56.6	-5.4 (7.1%)	-48.1 (63.6%)	-22.2 (29.3%)	-15.1 (68.0%)	-2.0 (9.0%)	-	-5.1 (23.1%)
NiP-Al-N_2	-23.8	93.9	-3.8 (3.3%)	-60.9 (51.7%)	-52.9 (45.0%)	-14.8 (27.9%)	-15.5 (29.3%)	-15.0 (28.3%)	-7.7 (14.5%)
NiP-Al-CO	-48.7	145.9	-3.7 (1.9%)	-110.8 (57.0%)	-80.0 (41.1%)	-19.6 (24.5%)	-24.8 (31.0%)	-23.9 (29.9%)	-11.7 (14.6%)
NiP-Al-NHC	-44.7	118.8	-15.1 (9.2%)	-101.6 (62.2%)	-46.7 (28.6%)	-22.9 (49.0%)	-7.2 (15.5%)	-4.2 (8.9%)	-12.4 (26.6%)
NiP-Ga-NH_3	-22.3	60.6	-5.4 (6.5%)	-53.2 (64.2%)	-24.3 (29.3%)	-16.7 (68.7%)	-2.3 (9.4%)	-	-5.3 (22.0%)
NiP-Ga-N_2	-24.8	92.5	-3.9 (3.3%)	-60.7 (51.7%)	-52.7 (45.0%)	-14.8 (28.1%)	-15.3 (29.1%)	-14.7 (27.8%)	-7.9 (15.0%)
NiP-Ga-CO	-49.3	143.3	-3.7 (1.9%)	-109.7 (57.0%)	-79.2 (41.1%)	-20.0 (25.3%)	-24.2 (30.6%)	-23.3 (29.4%)	-11.6 (14.7%)
NiP-Ga-NHC	-48.3	120.1	-15.1 (9.0%)	-105.4 (62.6%)	-47.9 (28.4%)	-24.0 (50.1%)	-7.1 (14.9%)	-4.1 (8.5%)	-12.7 (26.5%)
NiP-In-NH_3	-26.0	63.0	-5.4 (6.0%)	-57.8 (65.0%)	-25.8 (28.9%)	-17.6 (68.2%)	-2.7 (10.4%)	-	-5.5 (21.4%)
NiP-In-N_2	-28.9	92.7	-3.9 (3.2%)	-62.5 (51.4%)	-55.3 (45.4%)	-15.1 (27.3%)	-16.5 (29.8%)	-15.6 (28.2%)	-8.1 (14.6%)
NiP-In-CO	-53.2	139.9	-3.8 (2.0%)	-109.8 (56.9%)	-79.5 (41.2%)	-19.6 (24.7%)	-24.8 (31.2%)	-23.7 (29.9%)	-11.4 (14.3%)
NiP-In-NHC	-52.3	129.3	-15.7 (8.6%)	-114.5 (63.0%)	-51.4 (28.3%)	-25.5 (49.5%)	-8.0 (15.5%)	-4.5 (8.7%)	-13.5 (26.2%)

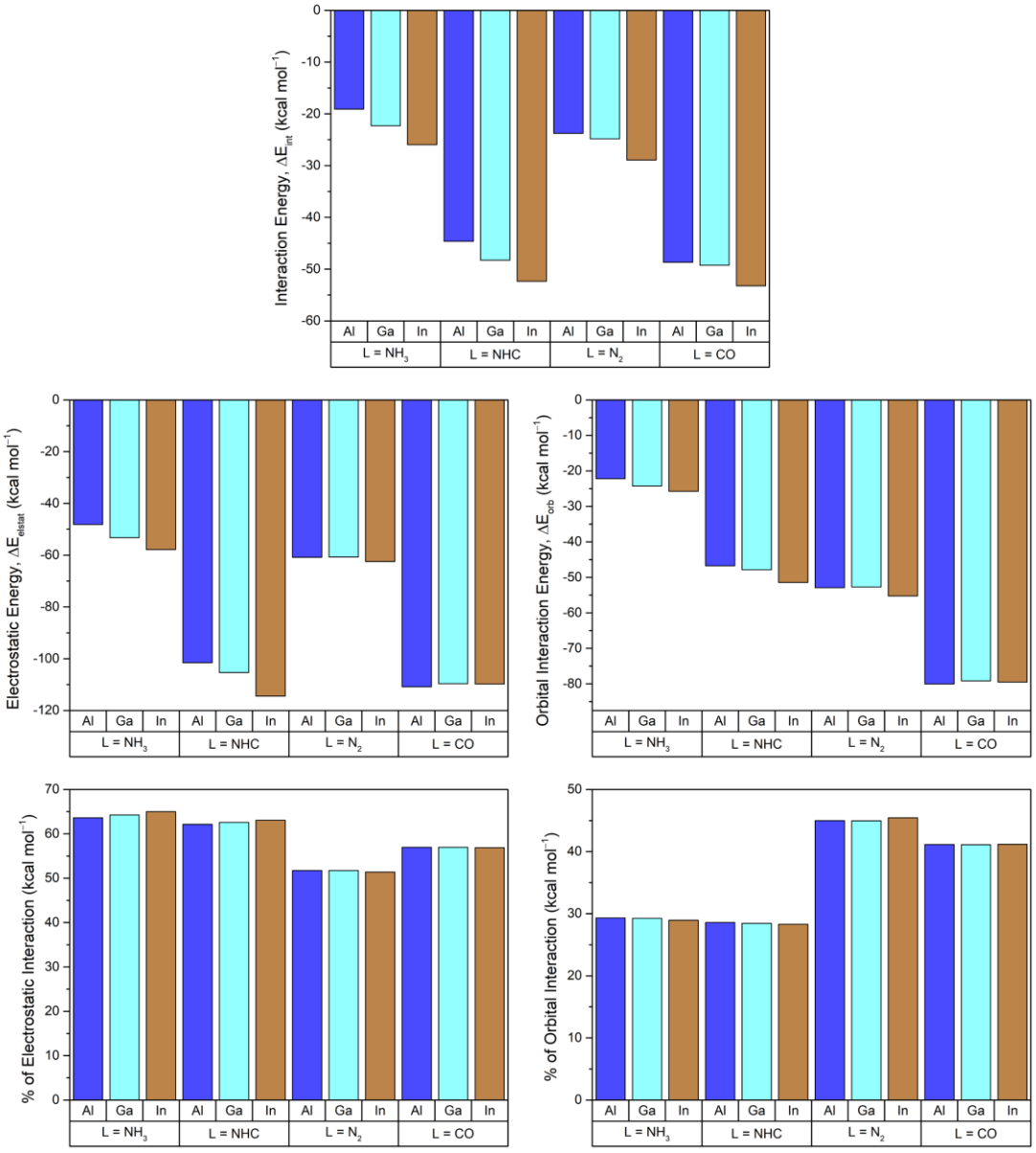

Figure 5.11: Interaction (ΔE_{int}), electrostatic (ΔE_{elstat}), and orbital interaction (ΔE_{orb}) energies of the phospha-metallatranes studied herein at the PBE0-D3/TZ2P level.

compares their relative contributions for the distinct Z = Al, Ga, In groups. The main NOCV pair and their corresponding deformation density plots and orbital interaction energies for the NiP-Z-CO systems are shown in Figure 5.12. Similar plots for the other phospha-nickelatrane systems are shown in Figure 5.13.

In all cases, the E_{int} values become more negative as Z becomes heavier. This is in line with our results obtained with the AIM approach, evidencing that the increase in

the M→Z interaction leads to a better M–L overlap. Regardless of the nature of the group 13 center, the largest E_{int} values are found for L = CO, which reaches -53.2 kcal mol^{-1} for the phospha-nickelaindatrane system. The ΔE_{int} decomposition reveals that the ΔE_{elstat} term is responsible for around 57% of the nickel-CO stabilizing contributions, while ΔE_{orb} sums to around 41%. Further partitioning of the ΔE_{orb} term indicates that Ni→CO π backbonding contributes to almost -50 kcal mol^{-1}, which represents around 60% of the stabilization due to orbital interaction. Indeed, as shown in Figure 5.12, two NOCV pairs are involved in the Ni→CO backbonding. On the other hand, the Ni←CO σ donation is around -20 kcal mol^{-1}. Inspection of the corresponding deformation density plots in Figure 5.12 reveals that the σ donation also increases electron density in the Ni···Z bonding region. However, this effect is not strong enough to overcompensate the Lewis basicity reduction of the Ni center due to delocalization effects involving the adjacent P centers, which results in weaker Ni···Z interaction.

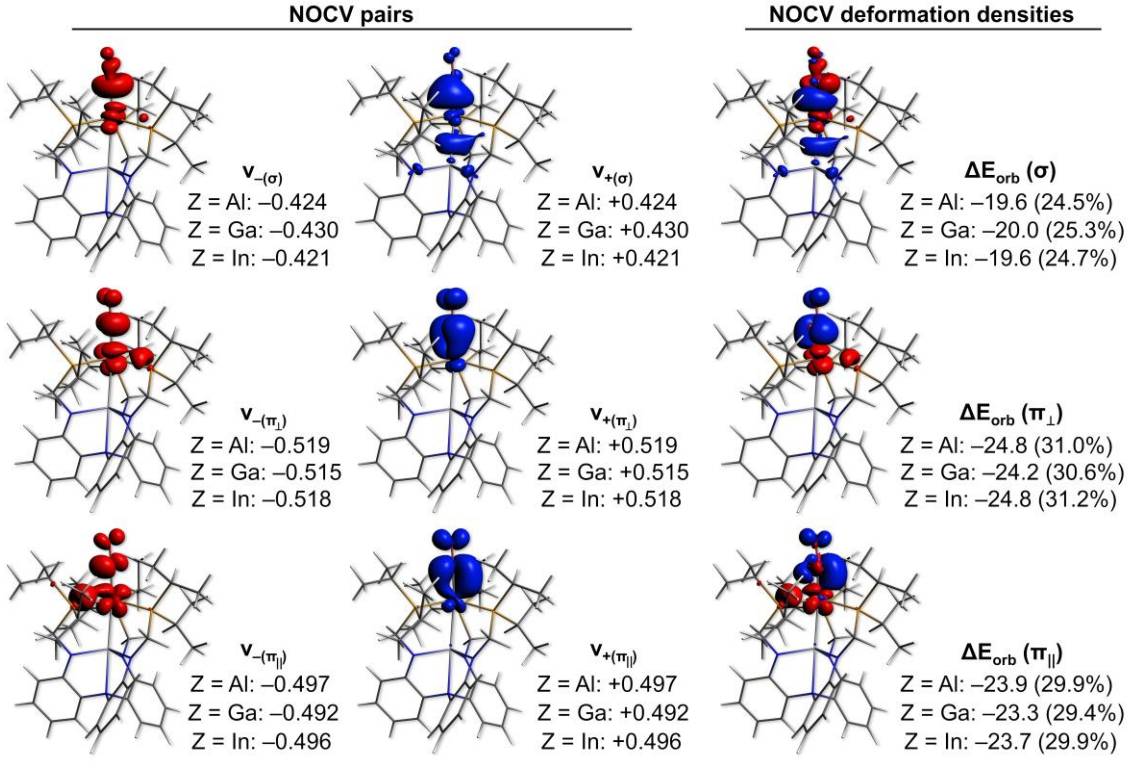

Figure 5.12: NOCV pairs and corresponding deformation density plots of the three main bonding configurations that contribute to the total ΔE_{orb} term in the EDA-NOCV description of the NiP-Z-CO (Z = Al, Ga, In) metallatranes. The NOCV eigenvalues and the orbital interaction energies (in kcal mol^{-1}) are also shown. The percentages of each contribution with respect to the total ΔE_{orb} term is shown in parenthesis. Isovalues: 0.0015 a.u. Charge flows from red to blue.

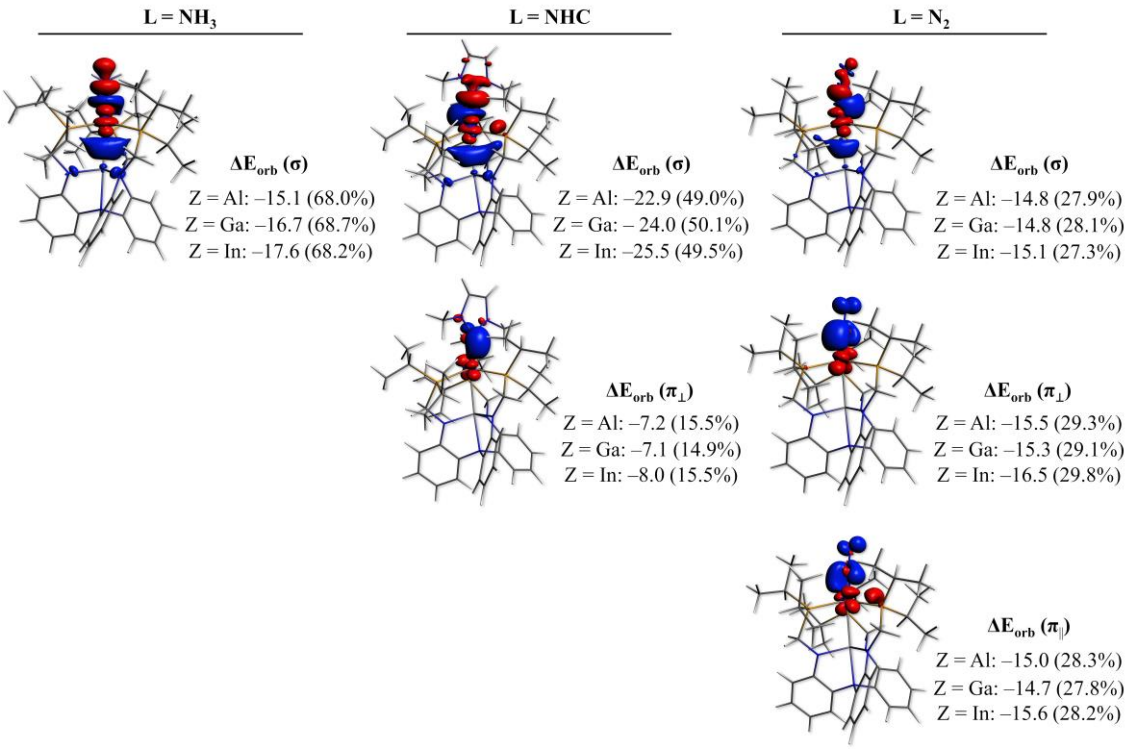

Figure 5.13: Deformation density plots and corresponding orbital interaction energies (in kcal mol^{-1}) of the three main bonding configurations that contribute to the total ΔE_{orb} term in the EDA-NOCV description of the NiP-Z-L (Z = Al, Ga, In; L = NH_3, NHC, N_2) metallatranes. The percentages of each contribution with respect to the total ΔE_{orb} term is shown in parenthesis. Isovalues: 0.0015 a.u. Charge flows from red to blue.

Compared to phospha-nickelatrane-carbonyl complexes, all the systems having NHC as the apical group have slightly smaller ΔE_{int} values, although further decomposition reveals that their interactions are quite distinct from L = CO. The NHC systems have considerably less Pauli repulsion and larger ΔE_{disp} energies, the latter reaching up to 10% of all the stabilizing contributions. The combination of these terms compensates their smaller ΔE_{orb} contributions. These come mainly from NHC→Ni σ donation, with only one dominant π backbonding NOCV term that contributes to merely around 15% of ΔE_{orb}.

In contrast to the previous cases, the ΔE_{int} of the NH_3 and N_2 complexes are in-between -19 kcal mol^{-1} (NiP-Al-NH_3) and -28.9 kcal mol^{-1} (NiP-In-N_2). While the M–L interactions for L = NH_3 are dominated by ΔE_{elstat} (ca. 65%), for L = N_2 the ΔE_{orb} contributions account for ~45%. The smaller orbital interactions for the NH_3 systems may be attributed to its pure σ donor nature. With respect to N_2, besides σ donation, contributions to ΔE_{orb} came from two NOCV pairs related to π backbonding are also at

play. By comparing the distinct NiP-Z-N_2 systems, it is possible to see that the π backbonding contributions increase for heavier group 13 atoms, in accordance with the tendencies observed for ΔE_{int}. Taken together, our results show that all four ligands form stabilizing interactions with the nickelatranes due to a combination of electrostatic, bonding, and dispersion interactions. These are increased if the heavier group 13 atoms are positioned in the bridgehead position, a strategy that becomes particularly relevant for the activation and functionalization [60] of less reactive species, such as N_2, which agrees with earlier experimental studies [15].

[5.6] Conclusions

Density functional theory calculations have been carried out to investigate the nature of intramolecular transannular interactions in group 13 metallatranes as a function of different equatorial (E), apical (L) and Lewis acidic groups (Z) (Scheme 5.1). Irrespective of the nature of the L groups, all the apically substituted metallatranes exhibit somewhat weaker M····Z interaction than that of the parent complexes. The extent of these transannular M····Z interactions depends to a large extent on the size and polarizability of the group 13 element (Z group). Furthermore, it should be noted that the strength of the transannular interaction plays a decisive role in governing the reactivity of the TM center in metallatranes. For example, the calculated reaction free energies (ΔG°) for binding of different Lewis bases are found to be more exergonic for the larger, more polarizable Lewis acidic In(III) ion than those for Al(III) or Ga(III) ions [56]. Therefore, such transannular interactions could be leveraged towards the binding of σ-donor or π acidic ligands to a given transition metal center. The quantum theory of atoms in molecules study also suggests the presence of considerable electron density (ρ) at the BCP of the M····Z bonds, which gradually increases as Z is varied down group 13 from Al to Ga to In. In addition, the calculated local electronic energy density (H(r)) values are found to be negative, indicating the covalent nature of the M····Z bonds. The EDA-NOCV analysis on few representative systems nicely captures the relative σ-donation and π-acceptance abilities of different ligands to metallatranes, as well as highlights the importance of the Lewis acidic group 13 center in promoting the binding of inert ligands, like N_2, to transition metal centers. We believe that our findings could contribute to the design of novel organometallic platforms for the binding and functionalization of a variety of ligand systems.

[5.7] Bibliography

[1] Parkin, G. A Simple Description of the Bonding in Transition-Metal Borane Complexes. *Organometallics*, 25(20):4744-4747, 2006.

[2] Hill, A. F. An Unambiguous Electron-Counting Notation for Metallaboratranes. *Organometallics*, 25(20):4741-4743, 2006.

[3] Shriver, D. F. Lewis Basicity of a Transition Metal. A Boron Trifluoride Adduct of Biscyclopentadienyltungsten Dihydride. *Journal of the American Chemical Society*, 85(21):3509-3510, 1963.

[4] Braunschweig, H., and Wagner, T. Zur Addition von Alkyldichlorboranen an Bis (η^5-cyclopentadienyl) dihydridowolfram. *Chemische Berichte*, 127(9):1613-1614, 1994.

[5] Burlitch, J. M., Leonowicz, M. E., Petersen, R. B., and Hughes, R. E. Coordination of metal carbonyl anions to triphenylaluminum,-gallium, and-indium and the crystal structure of tetraethylammonium triphenyl ((η^5-cyclopentadienyl)dicarbonyliron)aluminate(Fe-Al). *Inorganic Chemistry*, 18(4):1097-1105, 1979.

[6] Hill, A. F., Owen, G. R., White, A. J., and Williams, D. J. The Sting of the Scorpion: A Metallaboratrane. *Angewandte Chemie International Edition*, 38(18):2759-2761, 1999.

[7] Bontemps, S., Gornitzka, H., Bouhadir, G., Miqueu, K., and Bourissou, D. Rhodium(I) Complexes of a PBP Ambiphilic Ligand: Evidence for a Metal→Borane Interaction. *Angewandte Chemie International Edition*, 45(10):1611-1614, 2006.

[8] Kuzu, I., Krummenacher, I., Meyer, J., Armbruster, F., and Breher, F. Multidentate ligand systems featuring dual functionality. *Dalton Transactions*, (43):5836-5865, 2008.

[9] Fontaine, F. G., Boudreau, J., and Thibault, M. H. Coordination Chemistry of Neutral (L_n)–Z Amphoteric and Ambiphilic Ligands. *European Journal of Inorganic Chemistry*, 2008(35):5439-5454, 2008.

[10] Braunschweig, H., Dewhurst, R. D., and Schneider, A. Electron-Precise Coordination Modes of Boron-Centered Ligands. *Chemical Reviews*, 110(7):3924-3957, 2010.

[11] Bouhadir, G., Amgoune, A., and Bourissou, D. (2010). Phosphine-boranes and related ambiphilic compounds: synthesis, structure, and coordination to transition metals. In *Advances in Organometallic Chemistry*, Academic Press, Vol. 58, page. 1-107.

[12] Braunschweig, H., and Dewhurst, R. D. Transition metals as Lewis bases:"Z-type" boron ligands and metal-to-boron dative bonding. *Dalton Transactions*, 40(3):549-558, 2011.

[13] (a) Amgoune, A., and Bourissou, D. σ-Acceptor, Z-type ligands for transition metals. *Chemical Communications*, 47(3):859-871, 2011; (b) Bouhadir, G., and Bourissou, D. Complexes of ambiphilic ligands: reactivity and catalytic applications. *Chemical Society Reviews*, 45(4):1065-1079, 2016.

[14] (a) Kameo, H., and Nakazawa, H. Recent developments in the coordination chemistry of multidentate ligands featuring a boron moiety. *Chemistry–An Asian Journal*, 8(8):1720-1734, 2013; (b) Saha, K., Ramalakshmi, R., Borthakur, R., Gomosta, S., Pathak, K., Dorcet, V., Roisnel, T., Halet, J-F., and Ghosh, S. An Efficient Method for the Synthesis of Boratrane Complexes of Late Transition Metals. *Chemistry–A European Journal*, 23(72):18264-18275, 2017; (c) Schindler, T., Lux, M., Peters, M., Scharf, L. T., Osseili, H., Maron, L., and Tauchert, M. E. Synthesis and Reactivity of Palladium Complexes Featuring a Diphosphinoborane Ligand. *Organometallics*, 34(10):1978-1984, 2015; (d) Foreman, M. R. S. J., Hill, A. F., Ma, C., Tshabang, N., and White, A. J. Synthesis and ligand substitution reactions of κ^4-*B,S,S′,S″*-ruthenaboratranes. *Dalton Transactions*, 48(1):209-219, 2019; (e) Pang, K., Quan, S. M., and Parkin, G. Palladium complexes with Pd→B dative bonds: Analysis of the bonding in the palladaboratrane compound [κ^4-B(mim^{But})$_3$]Pd(PMe$_3$). *Chemical Communications*, (48):5015-5017, 2006; (f) Pang, K., Tanski, J. M., and Parkin, G. Reactivity of the Ni→B dative σ-bond in the nickel boratrane compounds [κ^4-B(mim^{But})$_3$]NiX (X= Cl, OAc, NCS, N$_3$): synthesis of a series of *B*-functionalized tris(2-mercapto-1-*tert*-butylimidazolyl)borato complexes, [YTm^{But}]NiZ.. *Chemical Communications*, (8):1008-1010, 2008; (g) Figueroa, J. S., Melnick, J. G., and Parkin, G. Reactivity of the Metal→ BX$_3$ Dative σ-bond: 1,2-Addition Reactions of the Fe→BX$_3$ Moiety of the Ferraboratrane Complex [κ^4-B(mim^{But})$_3$]Fe(CO)$_2$. *Inorganic Chemistry*, 45(18):7056-7058, 2006.

[15] Cammarota, R. C., and Lu, C. C. Tuning Nickel with Lewis Acidic Group 13 Metalloligands for Catalytic Olefin Hydrogenation. *Journal of the American Chemical Society*, 137(39):12486-12489, 2015.

[16] Sircoglou, M., Mercy, M., Saffon, N., Coppel, Y., Bouhadir, G., Maron, L., and Bourissou, D. Gold(I) Complexes of Phosphanyl Gallanes: From Interconverting to

Separable Coordination Isomers. *Angewandte Chemie International Edition*, 48(19):3454-3457, 2009.

[17] Derrah, E. J., Sircoglou, M., Mercy, M., Ladeira, S., Bouhadir, G., Miqueu, K., Maron, L. and Bourissou, D. Original Transition Metal→Indium Interactions upon Coordination of a Triphosphine−Indane. *Organometallics*, 30(4):657-660, 2011.

[18] Sircoglou, M., Bouhadir, G., Saffon, N., Miqueu, K., and Bourissou, D. A Zwitterionic Gold(I) Complex from an Ambiphilic Diphosphino−Alane Ligand. *Organometallics*, 27(8):1675-1678, 2008.

[19] Sircoglou, M., Saffon, N., Miqueu, K., Bouhadir, G., and Bourissou, D. Activation of M–Cl Bonds with Phosphine–Alanes: Preparation and Characterization of Zwitterionic Gold and Copper Complexes. *Organometallics*, 32(22):6780-6784, 2013.

[20] Devillard, M., Nicolas, E., Appelt, C., Backs, J., Mallet-Ladeira, S., Bouhadir, G., Slootweg, J. C.. Uhl, W., and Bourissou, D. Novel zwitterionic complexes arising from the coordination of an ambiphilic phosphorus–aluminum ligand to gold. *Chemical Communications*, 50(94):14805-14808, 2014.

[21] Saito, T., Hara, N., and Nakao, Y. Palladium Complexes Bearing Z-type PAlP Pincer Ligands. *Chemistry Letters*, 46(8):1247-1249, 2017.

[22] Moore, J. T., Smith, N. E., and Lu, C. C. Structure and dynamic NMR behavior of rhodium complexes supported by Lewis acidic group 13 metallatranes. *Dalton Transactions*, 46(17):5689-5701, 2017.

[23] (a) Moore, J. T., and Lu, C. C. Catalytic Hydrogenolysis of Aryl C–F Bonds Using a Bimetallic Rhodium–Indium Complex. *Journal of the American Chemical Society*, 142(27):11641-11646, 2020; (b) You, D., and Gabbaï, F. P. Tunable σ-accepting, Z-type ligands for organometallic catalysis. *Trends in Chemistry*, 1(5):485-496, 2019; (c) Takaya, J. Catalysis using transition metal complexes featuring main group metal and metalloid compounds as supporting ligands. *Chemical Science*, 12(6):1964-1981, 2021.

[24] Lai, Q., Cosio, M. N., and Ozerov, O. V. Ni complexes of an alane/tris (phosphine) ligand built around a strongly Lewis acidic tris(N-pyrrolyl) aluminum. *Chemical Communications*, 56(94):14845-14848, 2020.

[25] Devillard, M., Declercq, R., Nicolas, E., Ehlers, A. W., Backs, J., Saffon-Merceron, N., Bouhadir, G, Slootweg, J. C., Bourissou, D. A significant but Constrained

Geometry Pt→Al Interaction: Fixation of CO_2 and CS_2, Activation of H_2 and $PhCONH_2$. *Journal of the American Chemical Society*, 138(14):4917-4926, 2016.

[26] Takaya, J., and Iwasawa, N. Synthesis, Structure, and Catalysis of Palladium Complexes Bearing a Group 13 Metalloligand: Remarkable Effect of an Aluminum-Metalloligand in Hydrosilylation of CO_2. *Journal of the American Chemical Society*, 139(17):6074-6077, 2017.

[27] Rudd, P. A., Liu, S., Gagliardi, L., Young Jr, V. G., and Lu, C. C. Metal–Alane Adducts with Zero-Valent Nickel, Cobalt, and Iron. *Journal of the American Chemical Society*, 133(51):20724-20727, 2011.

[28] Vollmer, M. V., Xie, J., and Lu, C. C. Stable Dihydrogen Complexes of Cobalt(−I) Suggest an Inverse *trans*-Influence of Lewis Acidic Group 13 Metalloligands. *Journal of the American Chemical Society*, 139(19):6570-6573, 2017.

[29] Anderson, J. S., Rittle, J., and Peters, J. C. Catalytic conversion of nitrogen to ammonia by an iron model complex. *Nature*, 501(7465):84-87, 2013.

[30] Rudd, P. A., Planas, N., Bill, E., Gagliardi, L., and Lu, C. C. Dinitrogen Activation at Iron and Cobalt Metallalumatranes. *European Journal of Inorganic Chemistry*, 2013(22-23):3898-3906, 2013.

[31] Clouston, L. J., Bernales, V., Carlson, R. K., Gagliardi, L., and Lu, C. C. Bimetallic Cobalt–Dinitrogen Complexes: Impact of the Supporting Metal on N_2 Activation. *Inorganic Chemistry*, 54(19):9263-9270, 2015.

[32] Cammarota, R. C., Vollmer, M. V., Xie, J., Ye, J., Linehan, J. C., Burgess, S. A., Appel, A. M., Gagliardi, L., Lu, C. C. A Bimetallic Nickel–Gallium Complex Catalyzes CO_2 Hydrogenation via the Intermediacy of an Anionic d^{10} Nickel Hydride. *Journal of the American Chemical Society*, 139(40):14244-14250, 2017.

[33] Nesbit, M. A., Suess, D. L., and Peters, J. C. E–H Bond Activations and Hydrosilylation Catalysis with Iron and Cobalt Metalloboranes. *Organometallics*, 34(19):4741-4752, 2015.

[34] Harman, W. H., Lin, T. P., and Peters, J. C. A d^{10} Ni–(H_2) Adduct as an Intermediate in H–H Oxidative Addition across a Ni–B Bond. *Angewandte Chemie International Edition*, 53(4):1081-1086, 2014.

[35] Harman, W. H., and Peters, J. C. Reversible H_2 Addition across a Nickel–Borane Unit as a Promising Strategy for Catalysis. *Journal of the American Chemical Society*, 134(11):5080-5082, 2012.

[36] Suess, D. L., and Peters, J. C. H–H and Si–H Bond Addition to Fe≡NNR_2 Intermediates Derived from N_2. *Journal of the American Chemical Society*, 35(13):4938-4941, 2013.

[37] Zeng, G., and Sakaki, S. Unexpected Electronic Process of H_2 Activation by a New Nickel Borane Complex: Comparison with the Usual Homolytic and Heterolytic Activations. *Inorganic Chemistry*, 52(6):2844-2853, 2013.

[38] Weigend, F., and Ahlrichs, R. Balanced basis sets of split valence, triple zeta valence and quadruple zeta valence quality for H to Rn: Design and assessment of accuracy. *Physical Chemistry Chemical Physics*, 7(18):3297-3305, 2005.

[39] Zhao, Y., and Truhlar, D. G. The M06 suite of density functionals for main group thermochemistry, thermochemical kinetics, noncovalent interactions, excited states, and transition elements: two new functionals and systematic testing of four M06-class functionals and 12 other functionals. *Theoretical Chemistry Accounts*, 120(1):215-241, 2008.

[40] Weigend, F. Accurate Coulomb-fitting basis sets for H to Rn. *Physical Chemistry Chemical Physics*, 8(9):1057-1065, 2006.

[41] (a) Aghazada, S., Miehlich, M., Messelberger, J., Heinemann, F. W., Munz, D., and Meyer, K. A Terminal Iron Nitrilimine Complex: Accessing the Terminal Nitride through Diazo N−N Bond Cleavage. *Angewandte Chemie International Edition*, 58(51):18547-18551, 2019; (b) Müller, I., Munz, D., and Werncke, C. G. Reactions of Alkynes with Quasi-Linear 3d Metal(I) Silylamides of Chromium to Cobalt: A Comparative Study. *Inorganic Chemistry*, 59(14):9521-9537, 2020; (c) Fajardo Jr, J., and Peters, J. C Tripodal $P_3^XFe–N_2$ Complexes (X= B, Al, Ga): Effect of the Apical Atom on Bonding, Electronic Structure, and Catalytic N_2-to-NH_3 Conversion. *Inorganic Chemistry*, 60(2):1220-1227, 2021.

[42] Grimme, S., Antony, J., Ehrlich, S., and Krieg, H. A consistent and accurate ab initio parametrization of density functional dispersion correction (DFT-D) for the 94 elements H-Pu. *The Journal of Chemical Physics*, 132(15):154104, 2010.

[43] Glendening, E. D., Reed, A. E., Carpenter, J. E. and Weinhold, F. NBO Program 3.1, W. T. Madison, 1988.

[44] Reed, A. E., Curtiss, L. A., and Weinhold, F. Intermolecular Interactions from a Natural Bond Orbital, Donor-Acceptor Viewpoint. *Chemical Reviews*, 88(6):899-926, 1988.

[45] Frisch, M. J., Trucks, G. W., Schlegel, H. B., Scuseria, G. E., Robb, M. A., Cheeseman, J. R., Montgomery, J. A., Jr., Vreven, T., Kudin, K. N., Burant, J. C., Millam, J. M., Iyengar, S. S., Tomasi, J., Barone, V., Mennucci, B., Cossi, M., Scalmani, G., Rega, N., Petersson, G. A., Nakatsuji, H., Hada, M., Ehara, M., Toyota, K., Fukuda, R., Hasegawa, J., Ishida, M., Nakajima, T., Honda, Y., Kitao, O., Nakai, H., Klene, M., Li, X., Knox, J. E., Hratchian, H. P., Cross, J. B., Bakken, V., Adamo, C., Jaramillo, J., Gomperts, R., Stratmann, R. E., Yazyev, O., Austin, A. J., Cammi, R., Pomelli, C., Ochterski, J. W., Ayala, P. Y., Morokuma, K., Voth, G. A., Salvador, P. J., Dannenberg, J., Zakrzewski, V. G., Dapprich, S., Daniels, A. D., Strain, M. C., Farkas, O., Malick, D. K., Rabuck, A. D., Raghavachari, K., Foresman, J. B., Ortiz, J. V., Cui, Q., Baboul, A. G., Clifford, S., Cioslowski, J., Stefanov, B. B., Liu, G., Liashenko, A., Piskorz, P., Komaromi, I., Martin, R. L., Fox, D. J., Keith, T., Al- Laham, M. A., Peng, C. Y., Nanayakkara, A., Challacombe, M., Gill, P. M. W., Johnson, B., Chen, W., Wong, M. W., Gonzalez, C., and Pople, J. A. *Gaussian 03, Revision D.02*; Gaussian, Inc., Pittsburgh, PA, 2003.

[46] Bader, R. F. A Bond Path: A Universal Indicator of Bonded Interactions. *The Journal of Physical Chemistry A*, 102(37):7314-7323, 1998.

[47] Bader, Richard FW. A Quantum Theory of Molecular Structure and Its Applications. *Chemical Reviews*, 91(5): 893-928, 1991.

[48] Bader, R. F. W. (1990) Atoms in Molecules: a Quantum Theory; Oxford University Press: Oxford, U. K.

[49] Keith, T. A. AIMAll (Version 17.11.14, Professional); 2017 (http://aim.tkgristmill.com).

[50] (a) Mitoraj, M., and Michalak, A. Natural Orbitals for Chemical Valence as Descriptors of Chemical Bonding in Transition Metal Complexes. *Journal of Molecular Modeling*, 13(2):347-355, 2007; (b) Mitoraj, M. P., Michalak, A., and Ziegler, T. A combined charge and energy decomposition scheme for bond analysis. *Journal of Chemical Theory and Computation*, 5(4):962-975, 2009; (c) Zhao, L., von Hopffgarten, M., Andrada, D. M., and Frenking, G. Energy decomposition analysis. *Wiley Interdisciplinary Reviews: Computational Molecular Science*, 8(3): e1345, 2018.

[51] Te Velde, G. T., Bickelhaupt, F. M., Baerends, E. J., Fonseca Guerra, C., van Gisbergen, S. J., Snijders, J. G., and Ziegler, T. Chemistry with ADF. *Journal of Computational Chemistry*, 22(9):931-967, 2001.

[52] Lenthe, E. V., Baerends, E. J., and Snijders, J. G. Relativistic regular two-component Hamiltonians. *The Journal of Chemical Physics*, 99(6):4597-4610, 1993.

[53] (a) Mantina, M., Chamberlin, A. C., Valero, R., Cramer, C. J., and Truhlar, D. G. Consistent van der Waals Radii for the Whole Main Group. *The Journal of Physical Chemistry A*, 113(19):5806-5812, 2009; (b) Huheey, J. E.; Keiter, E. A. and Keiter, R. L. (1993) Inorganic Chemistry: Principles of Structure and Reactivity. 4th ed. Harper Collins College Publishers: New York.

[54] Cordero, B., Gómez, V., Platero-Prats, A. E., Revés, M., Echeverría, J., Cremades, E., Barragán, F., and Alvarez, S. Covalent radii revisited. *Dalton Transactions*, (21):2832-2838, 2008.

[55] (a) Pearson, R. G. Hard and Soft Acids and Bases. *Journal of the American Chemical Society*, 85(22):3533-3539, 1963; (b) Sivaev, I. B., and Bregadze, V. I. Lewis acidity of boron compounds. *Coordination Chemistry Reviews*, 270-271:75-88, 2014.

[56] Cammarota, R. C., Xie, J., Burgess, S. A., Vollmer, M. V., Vogiatzis, K. D., Ye, J., Linehan, J. C., Appel, A. M., Hoffmann, C., Wang, X., Yong, Jr, V. G, and Lu, C. C. Thermodynamic and kinetic studies of H_2 and N_2 binding to bimetallic nickel-group 13 complexes and neutron structure of a Ni (η^2-H_2) adduct. *Chemical Science*, 10(29):7029-7042, 2019.

[57] (a) Barnett, B. R., Moore, C. E., Chandrasekaran, P., Sproules, S., Rheingold, A. L., DeBeer, S., and Figueroa, J. S. Metal-only Lewis pairs between group 10 metals and Tl(I) or Ag(I): insights into the electronic consequences of Z-type ligand binding. *Chemical Science*, 6(12):7169-7178, 2015; (b) Lin, T. P., Nelson, R. C., Wu, T., Miller, J. T., and Gabbaï, F. P. Lewis acid enhancement by juxtaposition with an onium ion: the case of a mercury stibonium complex. *Chemical Science*, 3(4):1128-1136, 2012.

[58] (a) Stucke, N., Flöser, B. M., Weyrich, T., and Tuczek, F. Nitrogen Fixation Catalyzed by Transition Metal Complexes: Recent Developments. *European Journal of Inorganic Chemistry*, 2018(12):1337-1355, 2018; (b) Chalkley, M. J., Drover, M. W., and Peters, J. C. Catalytic N_2-to-NH_3 (or-N_2H_4) Conversion by Well-Defined Molecular Coordination Complexes. *Chemical Reviews*, 120(12):5582-5636, 2020.

[59] Cremer, D., and Kraka, E. Chemical Bonds Without Bonding Electron Density—Does the Difference Electron-Density Analysis Suffice for a Description of the Chemical Bond? *Angewandte Chemie International Edition in English*, 23(8):627-628, 1984.

[60] (a) Moret, M. E., and Peters, J. C. N_2 Functionalization at Iron Metallaboratranes. *Journal of the American Chemical Society*, 133(45):18118-18121, 2011; (b) Rempel, A., Mellerup, S. K., Fantuzzi, F., Herzog, A., Deißenberger, A., Bertermann, R., Engels, B., and Braunschweig, H. Functionalization of N_2 via Formal 1,3-Haloboration of a Tungsten(0) σ-Dinitrogen Complex. *Chemistry–A European Journal*, 26(68):16019-16027, 2020.